RESEARCH ARTICLE

Bundle-specific associations between white matter microstructure and Aβ and tau pathology in preclinical Alzheimer's disease

Alexa Pichet Binette[1,2]*, Guillaume Theaud[3], François Rheault[4], Maggie Roy[3], D Louis Collins[5], Johannes Levin[6,7], Hiroshi Mori[8], Jae Hong Lee[9], Martin Rhys Farlow[10], Peter Schofield[11,12], Jasmeer P Chhatwal[13], Colin L Masters[14], Tammie Benzinger[15,16], John Morris[15,16], Randall Bateman[15,16], John CS Breitner[1,2], Judes Poirier[1,2], Julie Gonneaud[2,17], Maxime Descoteaux[3], Sylvia Villeneuve[1,2,5]*, DIAN Study Group, PREVENT-AD Research Group

[1]Department of Psychiatry, Faculty of Medicine, McGill University, Montreal, Canada; [2]Douglas Mental Health University Institute, Montreal, Canada; [3]Sherbrooke Connectivity Imaging Laboratory (SCIL), Université de Sherbrooke, Sherbrooke, Canada; [4]Electrical Engineering, Vanderbilt University, Nashville, United States; [5]McConnell Brain Imaging Centre, Montreal Neurological Institute, Montreal, Canada; [6]Department of Neurology, Ludwig-Maximilians-Universität München, Munich, Germany; [7]German Center for Neurodegenerative Diseases (DZNE), Munich, Germany; [8]Department of Clinical Neuroscience, Osaka City University Medical School, Osaka, Japan; [9]Department of Neurology, Asan Medical Center, University of Ulsan College of Medicine, Seoul, Republic of Korea; [10]Department of Neurology, Indiana University, Bloomington, United States; [11]Neuroscience Research Australia, Sydney, Australia; [12]School of Medical Sciences, UNSW Sydney, Sydney, Australia; [13]Harvard Medical School, Massachusetts General Hospital, Boston, United States; [14]The Florey Institute of Neuroscience and Mental Health, University of Melbourne, Parkville, Australia; [15]Knight Alzheimer Disease Research Center, Washington University School of Medicine, St. Louis, United States; [16]Department of Neurology, Washington University School of Medicine, St. Louis, United States; [17]Normandie Univ, UNICAEN, INSERM, U1237, Institut Blood and Brain @ Caen-Normandie, Cyceron, Caen, France

***For correspondence:**
alexa.pichetbinette@mail.mcgill.ca (APB);
sylvia.villeneuve@mcgill.ca (SV)

Competing interest: See page 16

Funding: See page 16

Received: 09 September 2020
Accepted: 12 May 2021
Published: 13 May 2021

Reviewing editor: Morgan Barense, University of Toronto, Canada

Abstract Beta-amyloid (Aβ) and tau proteins, the pathological hallmarks of Alzheimer's disease (AD), are believed to spread through connected regions of the brain. Combining diffusion imaging and positron emission tomography, we investigated associations between white matter microstructure specifically in bundles connecting regions where Aβ or tau accumulates and pathology. We focused on free-water-corrected diffusion measures in the anterior cingulum, posterior cingulum, and uncinate fasciculus in cognitively normal older adults at risk of sporadic AD and presymptomatic mutation carriers of autosomal dominant AD. In Aβ-positive or tau-positive groups, lower tissue fractional anisotropy and higher mean diffusivity related to greater Aβ and tau burden in both cohorts. Associations were found in the posterior cingulum and uncinate fasciculus in preclinical sporadic AD, and in the anterior and posterior cingulum in presymptomatic mutation carriers. These results suggest that microstructural alterations accompany pathological accumulation as early as the preclinical stage of both sporadic and autosomal dominant AD.

Introduction

The progression of Alzheimer's disease (AD) includes a long asymptomatic phase, during which accumulating pathology is accompanied by various brain changes (**Jack et al., 2013**; **Sperling et al., 2011**). Beta-amyloid (Aβ) and tau proteins, the pathological hallmarks of the disease (**Duyckaerts et al., 2009**), start to accumulate decades before signs of cognitive impairment (**Bateman et al., 2012**; **Jansen et al., 2015**). Positron emission tomography (PET) can image both proteins in vivo (**Johnson et al., 2016**; **Klunk et al., 2004**; **Schöll et al., 2016**), and thus help in identifying the earliest brain changes associated with such pathologies. Aβ- and tau-PET tracer accumulate in distinct patterns of deposition that follows canonical brain networks/organization. Aβ develops a widespread pattern of deposition that recapitulates a default mode network-like pattern, accumulating early in the frontal and parietal lobes (**Mattsson et al., 2019**; **Villeneuve et al., 2015**). Tau accumulates in a more localized pattern that can start in the locus coeruleus before being detectable by tau-PET scans, followed by the medial temporal lobe in the preclinical phase of the disease, and spreading to the lateral temporal lobe and the rest of the brain in late stages (**Braak and Braak, 1991**; **Braak et al., 2011**). A prominent view is that pathology accumulates in functionally and/or structurally connected regions (**Franzmeier et al., 2019**; **Seeley et al., 2009**; **Sepulcre et al., 2017**; **Vogel et al., 2020**). Many studies have highlighted associations between Aβ- and tau-PET and brain functional activity early in the course of the disease (**Berron et al., 2020**; **Jones et al., 2017**; **Mormino et al., 2011**; **Sepulcre et al., 2017**). However, relations between pathology and white matter (WM) microstructure, as assessed by diffusion magnetic resonance imaging (MRI), remain elusive in preclinical AD. While WM degeneration is clearly apparent in the late symptomatic stages, how WM microstructure is affected early on in the disease process is less clear (**Sachdev et al., 2013**). Whole-brain diffusion MRI tractograms can represent the brain's WM architecture, but these are difficult to reconstruct because of extensive crossing of WM fibers and the complexity of tracking algorithms (**Rheault et al., 2020**). Recent advances in modeling and available algorithms have facilitated robust extraction of WM bundles with automated methods, thereby allowing their more precise investigation. As well, more specific measures have become available for analysis of WM (**Dyrby et al., 2014**). In particular, free-water (FW)-corrected diffusion tensor measures may offer better estimates of WM microstructure, yielding tissue-based fractional anisotropy and diffusivities after removing the FW contribution to each voxel (**Pasternak et al., 2009**).

We investigated diffusion-based measures of WM microstructure in bundles that connect cortical regions vulnerable to Aβ and tau deposition. We hypothesized that such bundles would show lower fractional anisotropy and higher diffusivity with more pathology as proxy of WM degeneration. We sought to expand upon the few studies linking preclinical AD pathology and WM microstructure and focused on bundles (defined a priori) connecting brain regions targeted early by AD pathology, notably the cingulum bundle (**Jacobs et al., 2018**). The latter is a large association bundle under the cingulate gyri that connects anterior to posterior cingulate regions and curves further into the parahippocampal gyri of the temporal lobe. This bundle is typically affected in symptomatic AD dementia (**Bubb et al., 2018**; **Jacobs et al., 2018**; **Kantarci et al., 2017**; **Roy et al., 2020**; **Wen et al., 2019**), and given its location, could be preferentially affected by Aβ, particularly in its anterior segment. Also of interest is the uncinate fasciculus, reported to be affected at the stage of mild cognitive impairment (**Mito et al., 2018**; **Roy et al., 2020**). This bundle connects parts of the limbic system, such as the hippocampus and amygdala, with the orbitofrontal cortex (**Von Der Heide et al., 2013**), brain regions thought to be key regions for tau and Aβ propagation, respectively (**van der Kant et al., 2020**). Our objective was to investigate associations between the microstructure in those bundles of interest and AD pathology in two cohorts of cognitively normal individuals at risk of AD, older adults at increased risk of sporadic AD and presymptomatic mutation carriers of autosomal dominant AD (ADAD).

Results

Approach and participants

Using state-of-the-art methods in diffusion MRI modeling, tractography, and tractometry, we aimed to better understand the associations between WM microstructure of key bundles in preclinical AD and deposition of Aβ and tau as measured by PET. We reasoned that the preclinical stage of AD should be the ideal point at which to study these questions, given that this is a period during which AD pathology is spreading but overall brain structure and function remain largely preserved. We therefore studied the preclinical stage of both late-onset sporadic AD and ADAD. Sporadic AD is the most common form of dementia, is multifactorial, and occurs most often in late life. ADAD is the rarer form of AD, caused by fully penetrant genetic mutations in PSEN1, PSEN2, or APP, that leads to Aβ accumulation up to 20 years prior to symptom onset (***Bateman et al., 2012***) and to onset of cognitive symptoms often in the 40s and early 50s. ADAD is considered a 'purer' form of preclinical AD since most mutation carriers do not exhibit age-associated co-pathologies. We studied a subset of 126 asymptomatic individuals at high risk of sporadic AD from the PRe-symptomatic EValuation of Experimental or Novel Treatments for AD (PREVENT-AD) cohort (***Breitner et al., 2016***) and 81 ADAD presymptomatic mutation carriers from the Dominantly Inherited Alzheimer's Network (DIAN) cohort (***Morris et al., 2012***). PREVENT-AD enrolls cognitively normal older adults at risk of sporadic AD given their parental or multiple-sibling family history of the disease. At the time of study, participants were on average 67.3 years of age, predominantly female, and highly educated (***Table 1***). Based on a threshold established previously using global cortical Aβ burden (***McSweeney et al., 2020***), 19% of the participants were considered Aβ-positive. We also considered the same proportion of participants with the highest entorhinal tau uptake to be tau-positive. DIAN enrolls adults from families with ADAD. Our focus was on presymptomatic mutation carriers, but analyses were also conducted in mutation non-carriers in order to rule out false-positive associations that could be due to off-target binding properties of the PET tracer. Mutation carriers were on average 34.5 years of age, while non-carriers were slightly older. Both groups had more than 50% female and were highly educated. For the DIAN cohort, we had access to Aβ-PET only, with 43% of the mutation carriers and none of the non-carriers classified as Aβ-positive (***Su et al., 2013***).

Table 1. Demographics.

	PREVENT-AD (n = 126)	DIAN mutation carriers (n = 81)	DIAN mutation non-carriers (n = 96)
Age (years)	67.3 ± 4.8 (68–83)	34.5 ± 9.9 (18–61)	39.3 ± 11.7 (19–69)
Sex F:M (%F)	94:32 (75%)	42:39 (52%)	56:40 (58%)
*APOE*4 carriers (%)	50 (40%)	24 (30%)	26 (27%)
Education (years)	15.2 ± 3.3 (7–24)	15.2 ± 3.0 (10–24)	15.1 ± 2.7 (10–26)
Handedness (n, % right-handed)	114 (90%)	69 (85%)	82 (85%)
Systolic blood pressure	129.0 ± 13.8 (100–164)	122.5 ± 10.2 (95–155)	123.5 ± 17.1 (90–190)
Diastolic blood pressure	74.0 ± 8.1 (60–96)	75.2 ± 8.8 (55–104)	77.1 ± 10.1 (60–110)
Global Aβ SUVR*	1.3 ± 0.3 (1.0–2.8)	1.6 ± 0.7 (0.8–3.7)	1.0 ± 0.1 (0.9–1.3)
Aβ-positive (%)	24 (19%)	35 (43%)	0 (0%)
Entorhinal tau SUVR	1.1 ± 0.1 (0.7–1.6)	NA	NA
Mini-Mental State Examination	28.8 ± 1.2 (24–30)	29.0 ± 1.3 (24–30)	29.2 ± 1.2 (25–30)
Estimated years to symptom onset†	−5.7 ± 7.6 (−20.8 to 16.8)	−13.6 ± 8.3 (−31.5 to 11.8)	−7.4 ± 12.5 (−28.8 to 21.4)

Values represent Mean ± SD (range). Participants with at least one ε4 allele were considered APOE4 positive. The Mini-Mental State Evaluation was administered at the same time as PET.

* Note that NAV4694 was used in PREVENT-AD and PIB was used in DIAN.

† Estimated years to symptom onset was calculated as the parent's age at dementia onset minus the age of the participant; four missing values in PREVENT-AD.

Aβ: beta-amyloid; APOE: apolipoprotein E; SUVR: standardized uptake value ratio; PET: positron emission tomography.

Methodology overview

We extracted FW-corrected diffusion tensor measures in bundles of interest. We reconstructed each individual's whole-brain tractogram using high angular resolution diffusion imaging and fiber orientation distribution functions (fODFs), and employed automated tools to isolate the anterior cingulum, the posterior cingulum, and the uncinate fasciculus (***Garyfallidis et al., 2018***; ***Rheault, 2020***; ***Wassermann et al., 2016***). Tractometry then generated bundle-specific quantification of five WM properties (***Cousineau et al., 2017***; ***Rheault et al., 2017***). These were tissue fractional anisotropy (FA_T), mean diffusivity (MD_T), axial diffusivity (AD_T), and radial diffusivity (RD_T). In each, 'T' represents tissue in these FW-corrected diffusion tensor measures. We also report the FW index, which is thought to reflect a measure of neuroinflammation (***Pasternak et al., 2009***). To investigate the relationships with AD pathology, we focused on typical measures of Aβ- and tau-PET, which is a global cortical Aβ burden (in PREVENT-AD and DIAN) and entorhinal tau tracer uptake (in PREVENT-AD only).

We first evaluated the partial correlations between WM microstructure and pathology at the whole group level, controlling for age, sex, and bundle volume. We then repeated these analyses while restricting them to participants with (Aβ-positive or tau-positive) and without (Aβ-negative or tau-negative) pathology. The analysis conducted in Aβ-positive or tau-positive groups was especially important for the PREVENT-AD cohort since participants free from pathology might never develop AD. In complementary analyses, to investigate whether the associations would be independent from gray matter (GM) neurodegeneration, we further added GM volume in brain regions connected by our bundles of interest as covariates in the regression models. Lastly, we evaluated whether similar associations could be detected with typical diffusion tensor measures, that is, FA, MD, AD, and RD (not corrected for FW).

An overview of the processing steps is shown in ***Figure 1*** and can be summarized as follows: in three a priori WM bundles of interest extracted in the left and right hemisphere from each participant's tractogram, we evaluated associations between five related microstructure measures and AD pathology measured with PET (global cortical Aβ and entorhinal tau). We analyzed all five WM microstructure measures to detect whether a consistent pattern of associations across measures emerges rather than focusing on one given measure.

Associations in the uncinate fasciculus and posterior cingulum in PREVENT-AD Aβ-positive and tau-positive groups

In PREVENT-AD, at the level of the whole group, there were no associations between global cortical Aβ or entorhinal tau burden with any of the WM microstructure measures across the three bundles of interest (***Figure 2—source data 1***, ***Figure 3—source data 1***). Associations were detected only in the participants considered as Aβ-positive or tau-positive. In the Aβ-positive group, controlling for age, sex, and bundle volume, lower FA_T, higher MD_T, and higher RD_T in the left posterior cingulum and in the uncinate fasciculus were related to greater cortical Aβ burden (***Figure 2***, ***Figure 2—source data 1***). Similar associations were present in the right uncinate fasciculus at trend level ($p=0.06$ for FA_T, MD_T, and RD_T). Further, in the posterior cingulum, tau-positive participants displayed the same pattern of associations aforementioned; in this group, lower FA_T, higher MD_T, and higher RD_T in the left posterior cingulum related to greater entorhinal tau-PET tracer binding (***Figure 3***, ***Figure 3—source data 1***). Associations in the right posterior cingulum in tau-positive participants were trend level ($p=0.06$ for FA_T, MD_T, and RD_T).

In the anterior cingulum, there were no associations between WM measures and pathology in either Aβ-positive or tau-positive participants (***Figures 2D–3D***). No association was found in the Aβ- and tau-negative groups.

Associations in anterior and posterior cingulum in DIAN mutation carriers

In DIAN mutation carriers, associations were found at the group level between global Aβ burden and WM microstructure in the anterior cingulum, following the same pattern of associations as in PREVENT-AD. As such, lower FA_T, higher MD_T, and higher RD_T related to greater cortical Aβ across all mutation carriers (partial $R = -0.27$ for FA_T and 0.28 for MD_T and RD_T, $p=0.02$; ***Figure 4—source data 1***), but associations were higher when restricted to the Aβ-positive participants (***Figure 4A–D***).

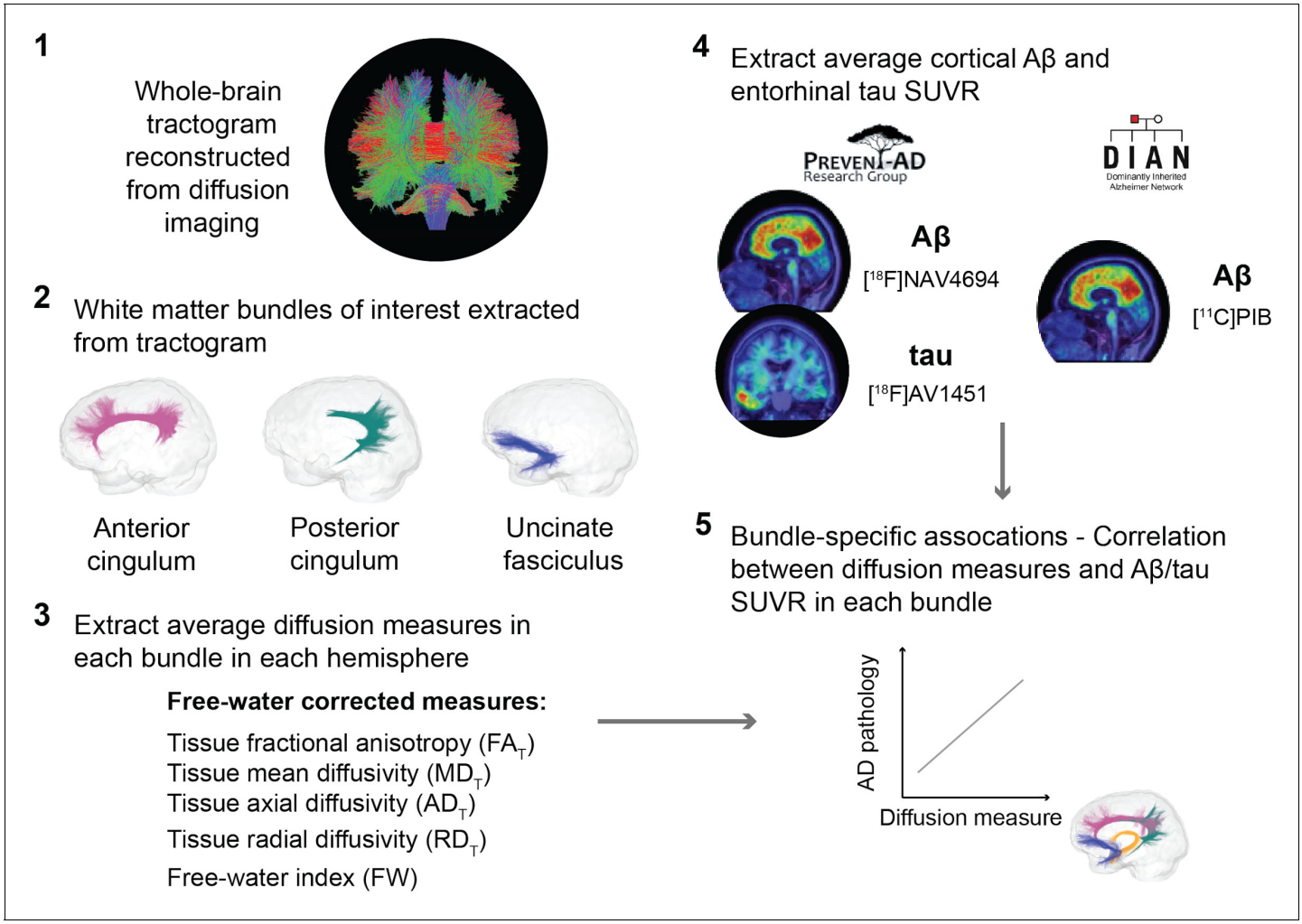

Figure 1. Overview of the processing steps. PREVENT-AD and DIAN participants were processed following the same pipeline. Whole-brain tractogram was reconstructed using the TractoFlow Atlas-Based Segmentation pipeline, and automated bundle extraction tools were used to extract the bundles of interest in each hemisphere. Free-water-corrected tensor measures were calculated for each bundle. Associations between white matter microstructure and global Aβ and entorhinal tau PET were then investigated. Aβ: beta-amyloid; PET: positron emission tomography; SUVR: standardized uptake value ratio.

Associations in Aβ-positive participants were also found in the right posterior cingulum (***Figure 4B–E***). Focusing only on the Aβ-negative group, microstructure measures in the posterior cingulum were associated with global cortical Aβ in the same directions as in the Aβ-positive group (partial $R = -0.31$ for FA_T and 0.31 for MD_T and RD_T, $p=0.01$). Of note, we did not find any associations between bundle microstructure and pathology in mutation non-carriers.

Effect of GM atrophy on microstructure-pathology associations

We further wanted to evaluate whether significant associations between bundle microstructure and pathology in Aβ-positive or tau-positive participants were affected by GM atrophy. To do so, we added GM volume specifically in brain regions connected by the bundle of interest as an additional covariate. Partial correlations were thus controlled for age, sex, bundle volume, and GM volume. GM volume of the following regions were considered: the anterior and posterior cingulate cortex for the anterior cingulum, the precuneus and the parahippocampal gyrus for the posterior cingulum, and the medial orbitofrontal cortex and the parahippocampal gyrus for the uncinate fasciculus. In both PREVENT-AD and DIAN, further adjusting for GM volume did not change the significance of the microstructure measures in neither the anterior cingulum nor the uncinate fasciculus. The only

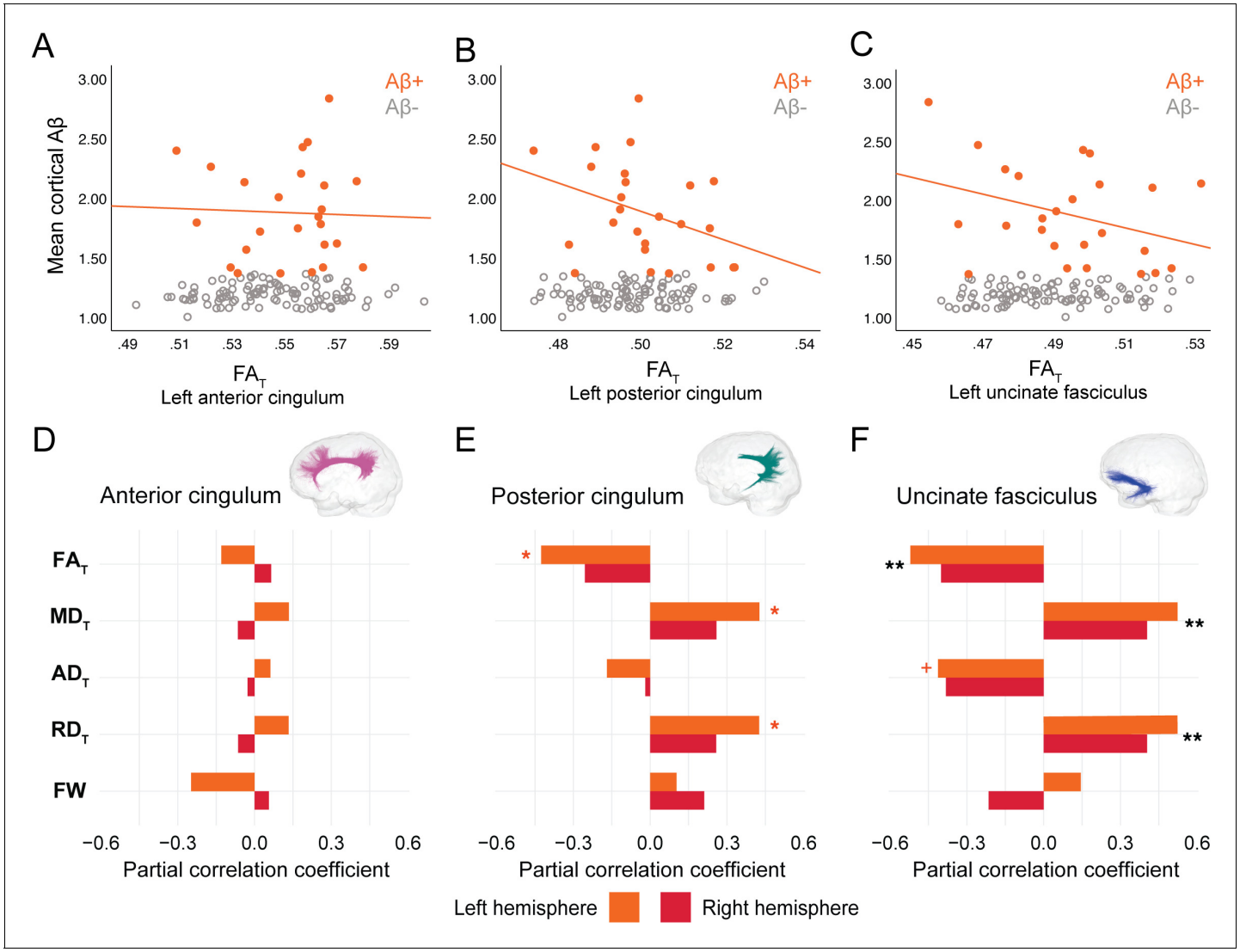

Figure 2. Associations between diffusion measures and Aβ burden in Aβ-positive PREVENT-AD participants. (**A–C**) Bivariate associations between FA_T and global cortical Aβ in each bundle in the left hemisphere to show examples of raw values in PREVENT-AD. Data are represented for the full sample, with Aβ-positive in orange (our group of interest) and Aβ-negative in gray. (**D–F**) Partial correlations between diffusion measures (average diffusion measure in the bundle) and global cortical Aβ-PET controlling for age, sex, and bundle volume (divided by total intracranial volume) were performed in PREVENT Aβ-positive participants. Partial correlation coefficient for each diffusion measure in the right and left bundles is reported as bar graphs. Black asterisks highlight that associations are significant in both hemispheres, otherwise the color of the symbol matches the hemisphere where the association is significant. *p=0.05; ** 0.05 > p > 0.001; +p=0.06. See also ***Figure 2—source data 1***. Aβ: beta-amyloid; FA_T: tissue fractional anisotropy; MD_T: tissue mean diffusivity; AD_T: tissue axial diffusivity; RD_T: tissue radial diffusivity; FW: free-water index; PET: positron emission tomography.
The online version of this article includes the following source data for figure 2:

Source data 1. Associations between microstructure and beta-amyloid–positron emission tomography (Aβ-PET) in PREVENT-AD.

bundle where atrophy changed the original associations was the posterior cingulum, with GM volume of the precuneus as a covariate. In both PREVENT-AD and DIAN, in models including volume of the precuneus, microstructure properties were no longer related to pathology. When volume of the parahippocampal gyrus was a covariate in the models of the posterior cingulum, microstructure associations were unchanged compared to the initial analyses, with the exception of the ones with Aβ burden in PREVENT-AD (the contribution of diffusion measures became marginal, changing from p=0.05 to p=0.06). In complementary analyses, we evaluated whether GM volume related to Aβ- and tau-PET controlling for age and sex. The main significant associations were in the right precuneus or posterior cingulate in PREVENT-AD and in the right posterior cingulate in DIAN (***Table 2***).

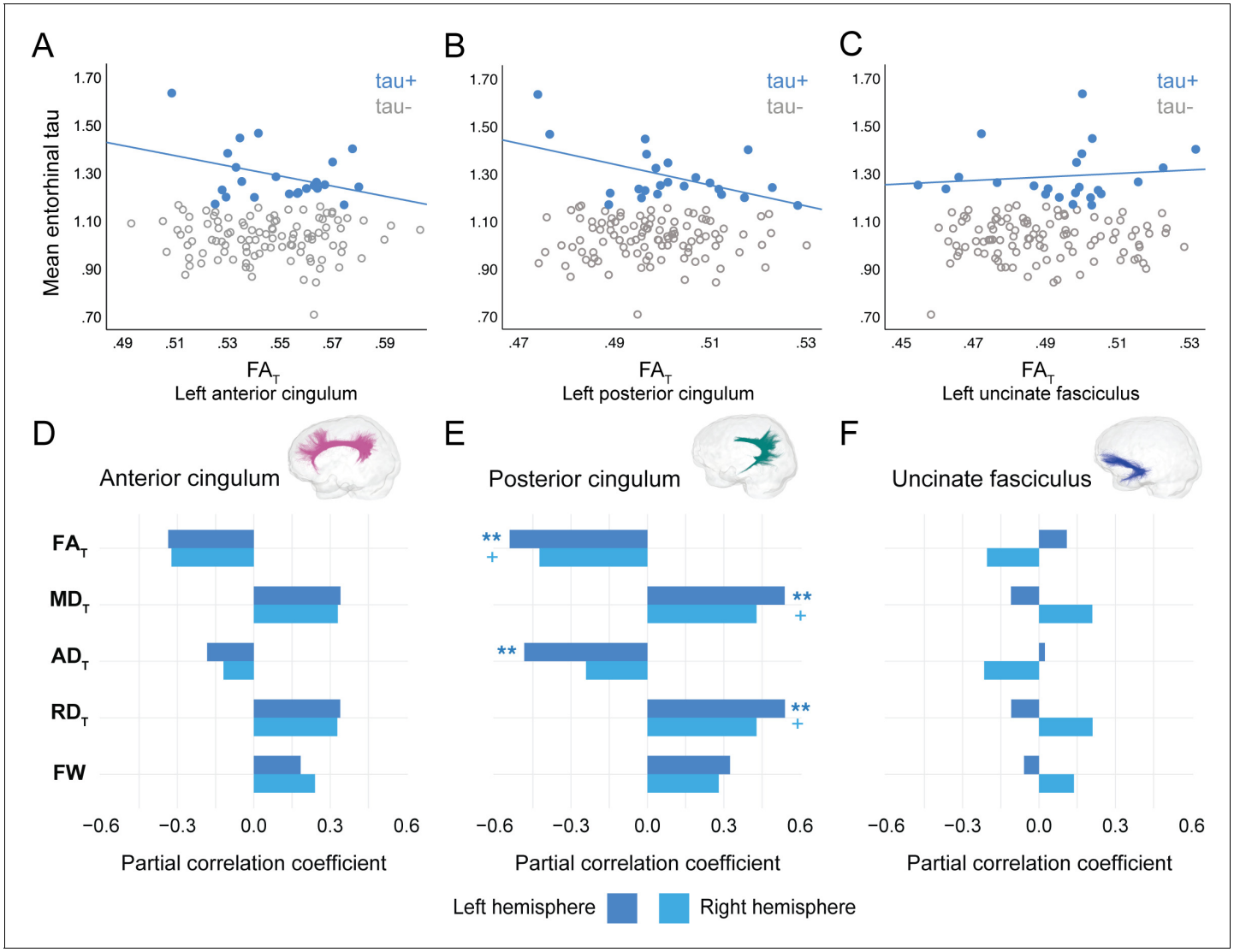

Figure 3. Associations between diffusion measures and entorhinal tau burden in tau-positive PREVENT-AD participants. (**A–C**) Bivariate associations between FA_T and entorhinal tau in each bundle in the left hemisphere to show examples of raw values in PREVENT-AD. Data are represented for the full sample, with tau-positive in blue (our group of interest) and tau-negative in gray. (**D–F**) Partial correlations between diffusion measures (average diffusion measure in the bundle) and entorhinal tau-PET controlling for age, sex, and bundle volume (divided by total intracranial volume) were performed in PREVENT tau-positive participants. Partial correlation coefficient for each diffusion measure in the right and left bundles is reported as bar graphs. The color of the symbol on the bar graphs matches the hemisphere where the association is significant. *p=0.05; ** 0.05 > p > 0.001; +p=0.06. See also ***Figure 3—source data 1***. FA_T: tissue fractional anisotropy; MD_T: tissue mean diffusivity; AD_T: tissue axial diffusivity; RD_T: tissue radial diffusivity; FW: free-water index; PET: positron emission tomography.

The online version of this article includes the following source data for figure 3:

Source data 1. Associations between microstructure and tau-positron emission tomography (tau-PET) in PREVENT-AD.

Importance of advanced FW measures to these results

To evaluate the sensitivity of FW-corrected measures over the typical tensor measures, we tested whether similar associations with pathology exist with FA, MD, AD, and RD (i.e., not corrected for FW). Except for FA, which gave similar results to FA_T, MD, RD, and AD were not associated with pathology in any bundle (***Table 3***), suggesting that FW-corrected measures capture subtle WM microstructure alterations not always detectable with more classical diffusion tensor imaging (DTI) measures.

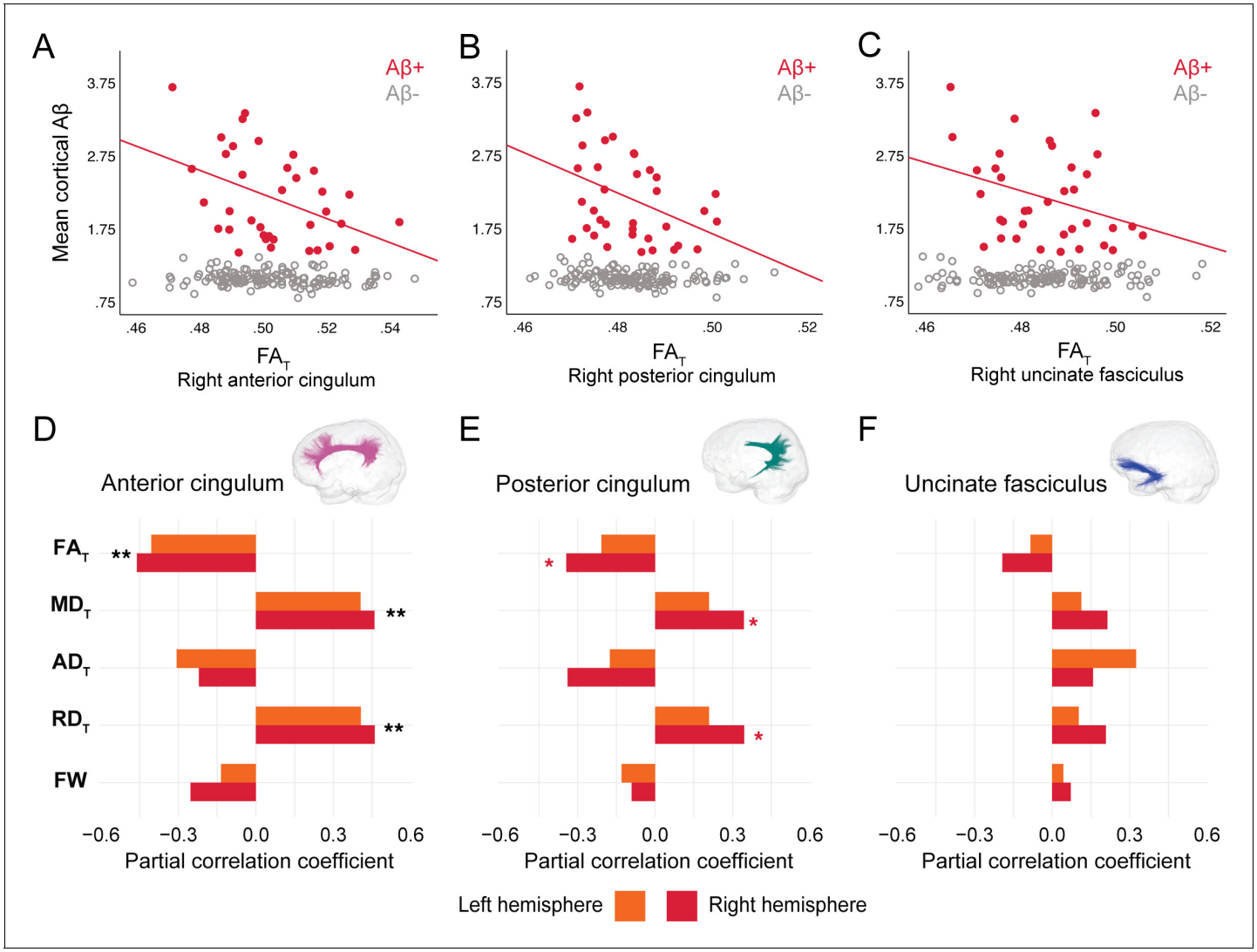

Figure 4. Associations between diffusion measures and Aβ burden in Aβ-positive DIAN mutation carriers. (**A–C**) Bivariate associations between FA_T and global cortical Aβ in each bundle in the left hemisphere to show examples of raw values in DIAN. Data are represented for the full sample, with Aβ-positive in red (our group of interest) and Aβ-negative in gray. (**D–F**) Partial correlations between diffusion measures (average diffusion measure in the bundle) and global cortical Aβ-PET controlling for age, sex, and bundle volume (divided by total intracranial volume) were performed in DIAN Aβ-positive participants. Partial correlation coefficient for each diffusion measure in the right and left bundles is reported as bar graphs. Black asterisks highlight that associations are significant in both hemispheres, otherwise the color of the symbol matches the hemisphere where the association is significant *p=0.05; ** 0.05 > p > 0.001. See also ***Figure 4—source data 1***. Aβ: beta-amyloid; FA_T: tissue fractional anisotropy; MD_T: tissue mean diffusivity; AD_T: tissue axial diffusivity; RD_T: tissue radial diffusivity; FW: free-water index; PET: positron emission tomography.
The online version of this article includes the following source data for figure 4:

Source data 1. Associations between microstructure and beta-amyloid–positron emission tomography (Aβ-PET) in DIAN.

Discussion

The notion that AD pathology accumulates in connected regions in the brain has foundations in rodent models (***Ahmed et al., 2014***; ***Jucker and Walker, 2018***; ***Palop and Mucke, 2010***), and it is gaining credence in human neuroimaging studies. It is striking how pathology deposit in structurally or functionally connected regions (***Franzmeier et al., 2020***; ***Seeley et al., 2009***; ***Sepulcre et al., 2016***; ***Vogel et al., 2020***). However, there is limited evidence on how WM microstructure in bundles linking those key pathology regions is affected in the early phases of AD. Combining Aβ- and tau-PET with recent advanced diffusion imaging analyses, we investigated WM microstructure in bundles (selected a priori) that connect key AD brain regions with Aβ and tau deposition. Our aim here was

Table 2. Associations between gray matter volume and Aβ- and tau-PET in PREVENT-AD and DIAN.

	PREVENT-AD Aβ-positive		PREVENT-AD Tau-positive		DIAN Aβ-positive	
	$R_{partial}$	p-value	$R_{partial}$	p-value	$R_{partial}$	p-value
Left hemisphere						
Anterior cingulate	−0.239	0.271	0.032	0.891	−0.207	0.248
Posterior cingulate	−0.116	0.598	−0.156	0.5	−0.252	0.156
Precuneus	−0.265	0.221	**−0.439**	0.047	−0.307	0.082
Parahippocampal gyrus	0.114	0.605	−0.073	0.753	0.079	0.661
Medial orbitofrontal cortex	−0.468	0.024	−0.197	0.392	−0.174	0.334
Right hemisphere						
Anterior cingulate	−0.335	0.118	−0.085	0.713	−0.133	0.461
Posterior cingulate	−0.342	0.111	**−0.546**	0.01	**−0.352**	0.045
Precuneus	**−0.468**	0.024	**−0.491**	0.024	−0.287	0.105
Parahippocampal gyrus	0.014	0.948	−0.213	0.355	0.16	0.373
Medial orbitofrontal cortex	−0.358	0.093	−0.237	0.301	0.014	0.94

$R_{partial}$ and p-values from regression models investigating associations between gray matter volume (divided by total intracranial volume; independent variable) and pathology (dependent variable) in Aβ-positive or tau-positive participants in PREVENT-AD and DIAN. Models included age and sex as covariates.

Aβ: beta-amyloid; PET: positron emission tomography.

not to test the spreading hypothesis per se, but, assuming that this hypothesis is correct, to focus on local effects of microstructure alterations and the presence of AD pathology in the preclinical stage of the disease. We investigated diffusion–PET associations in a cohort of asymptomatic older adults at risk of AD dementia due to their family history of sporadic AD and presymptomatic ADAD mutation carriers. In both cohorts, we found lower FA_T, higher MD_T, and higher RD_T were related to greater pathology. In PREVENT-AD, associations were found in the uncinate fasciculus and the posterior cingulum, whereas in DIAN associations were found in the anterior and posterior segments of the cingulum. Furthermore, in the PREVENT-AD the associations were restricted to participants with significant AD pathology. These results suggest that significant levels of Aβ- and tau-PET tracer binding are associated with WM neurodegeneration both in the preclinical phase of sporadic AD and ADAD.

Our 'bundle-specific' approach through tractography and tractometry suggests topographical relationships between pathology and WM microstructural alterations in the early stage of AD and complements the typical approach of voxel-wise analyses (***Harrison et al., 2020***; ***Zhang et al., 2019***). Using more precise tissue measures with FW corrected as opposed to classical diffusion tensor measures strengthened our findings, further highlighting the relevance of novel methods. Most of the models proposing a cascade of events over the course of AD have not included WM alterations (***Iturria-Medina et al., 2016***; ***Jack et al., 2013***). One exception being a recent model in ADAD that included diffusivity, with higher MD being detectable 5–10 years prior to symptom onset (***Araque Caballero et al., 2018***). Although the current study design precludes us from staging when microstructure starts to change, our findings suggest that WM degeneration already occurs with early pathology accumulation prior to symptom onset both in the sporadic and the autosomal dominant forms of AD.

The observed associations follow the classical pattern of degeneration that is characterized by lower anisotropy and higher diffusivity, representing loss of coherence in the WM microstructure with AD progression (***Badea et al., 2016***; ***Caso et al., 2016***; ***Sexton et al., 2011***). This pattern of WM degeneration develops invariably along the AD spectrum (***Amlien and Fjell, 2014***; ***Pereira et al., 2019***), with changes often becoming detectable only in the mild cognitive impairment and dementia stages (***Mito et al., 2018***; ***Song et al., 2018***; ***Wang et al., 2019***; ***Wen et al., 2019***), and rarely in Aβ-positive cognitively normal participants (***Rieckmann et al., 2016***; ***Vipin et al., 2019***). Our results further emphasize that in presymptomatic populations associations start to be

Table 3. Associations between typical tensor measures and Aβ- and tau-PET in PREVENT-AD and DIAN.

	PREVENT-AD					
Aβ-positive						
	Anterior cingulum		Posterior cingulum		Uncinate fasciculus	
	$R_{partial}$	p-value	$R_{partial}$	p-value	$R_{partial}$	p-value
Left hemisphere						
FA	−0.128	0.571	−0.429	0.046	−0.526	0.012
MD	0.022	0.923	0.18	0.424	0.32	0.147
AD	−0.106	0.637	−0.315	0.153	−0.305	0.168
RD	0.081	0.721	0.305	0.168	0.448	0.037
Right hemisphere						
FA	−0.021	0.927	−0.3	0.175	−0.566	0.006
MD	−0.048	0.831	0.131	0.56	0.078	0.729
AD	−0.067	0.766	−0.102	0.651	−0.381	0.08
RD	−0.019	0.931	0.221	0.322	0.344	0.116
Tau-positive						
	Anterior cingulum		Posterior cingulum		Uncinate fasciculus	
	$R_{partial}$	p-value	$R_{partial}$	p-value	$R_{partial}$	p-value
Left hemisphere						
FA	−0.465	0.039	−0.523	0.018	0.108	0.65
MD	0.511	0.021	0.396	0.084	0.054	0.821
AD	0.112	0.639	0.082	0.731	0.206	0.384
RD	0.546	0.013	0.465	0.039	−0.014	0.953
Right hemisphere						
FA	−0.461	0.041	−0.487	0.029	−0.399	0.081
MD	0.416	0.068	0.372	0.106	0.211	0.372
AD	0.012	0.959	0.157	0.508	−0.011	0.965
RD	0.495	0.027	0.444	0.05	0.311	0.182
	DIAN					
Aβ-positive						
	Anterior cingulum		Posterior cingulum		Uncinate fasciculus	
	$R_{partial}$	p-value	$R_{partial}$	p-value	$R_{partial}$	p-value
Left hemisphere						
FA	−0.373	0.035	−0.192	0.293	−0.031	0.868
MD	0.15	0.413	−0.051	0.783	−0.015	0.935
AD	−0.196	0.283	−0.226	0.213	−0.067	0.716
RD	0.318	0.076	0.049	0.79	0.021	0.91
Right hemisphere						
FA	−0.452	0.009	−0.4	0.023	−0.35	0.049
MD	0.122	0.505	−0.002	0.991	0.108	0.558
AD	−0.239	0.188	−0.219	0.229	−0.098	0.595
RD	0.335	0.061	0.146	0.426	0.209	0.251

$R_{partial}$ and p-values from regression models investigating associations between each tensor measure (average diffusion measure in the bundle; independent variable) and pathology (dependent variable) in PREVENT-AD Aβ-positive or tau-positive participants and DIAN Aβ-positive participants. Models included age, sex, bundle volume (divided by total intracranial volume) as covariates.

Aβ: beta-amyloid; FA: fractional anisotropy; MD: mean diffusivity; AD: axial diffusivity; RD: radial diffusivity; PET: positron emission tomography.

detectable in individuals with high amount of pathology. In effect, most of the microstructure-pathology associations were restricted to the Aβ-positive or tau-positive participants. We should note that in the asymptomatic stage there is also evidence of WM alterations opposing the typical degeneration pattern, suggesting a possible biphasic relationship over the course of the disease (**Fortea et al., 2010**; **Montal et al., 2018**; **Wearn et al., 2020**). For instance, hypertrophy, glial activation, neuronal or glial swelling have been attributed higher anisotropy and lower diffusivity in the asymptomatic phase (**Fortea et al., 2010**; **Montal et al., 2018**). The biomarker status (i.e., Aβ-positive or negative) might be important to disentangle such early processes (**Dong et al., 2020**; **Racine et al., 2014**). Not dichotomizing by pathology status might obscure some associations in the early disease stages, as shown here.

The bundle that was consistently affected in participants with high pathology in both cohorts was the posterior cingulum, a key bundle in AD (**Agosta et al., 2011**; **Caso et al., 2016**; **Zhuang et al., 2012**). The posterior cingulum is certainly altered in the symptomatic stage, and diffusivity in this bundle has also shown to be related to tau accumulation in preclinical individuals (**Jacobs et al., 2018**). In the PREVENT-AD cohort, the posterior segment of the bundle was the only region where tau-positive participants presented WM degeneration with greater entorhinal tau. In DIAN, although we did not have tau-PET, we hypothesize that the associations found in Aβ-positive in the posterior cingulum would be present with tau since mutation carriers harbor elevated tau binding in the precuneus (**Gordon et al., 2019**). In an attempt to explore whether associations were independent of atrophy in brain regions connected the bundles of interest, we also controlled for GM volume in such regions. In both cohorts, the precuneus is the only region where, when added as a covariate, microstructure was no longer related to pathology. Such finding might suggest that this critical region in AD pathophysiology might already be further along the degeneration process, with white and GM being affected. Our results both in preclinical sporadic and ADAD corroborate the idea that the precuneus/posterior cingulum, more largely part of the posterior default mode network or posterior-medial system, is a critical area in the cascading events of AD (**Berron et al., 2020**; **Jones et al., 2016**).

In DIAN, the other bundle where Aβ and WM measures were related was the anterior cingulum, another bundle connecting key regions where Aβ accumulates. In line with these results, similar associations have been found in DIAN using CSF Aβ (**Finsterwalder et al., 2020**). On the other hand, in PREVENT-AD, the strongest associations with Aβ were detected in the uncinate fasciculus. This bundle has an interesting anatomy, connecting regions at the intersection of both Aβ (frontal lobe) and tau (temporal lobe) deposition patterns in sporadic AD. We speculate that the particular localization of the uncinate fasciculus with regards to Aβ and tau deposition might confer early vulnerability to pathological insults. Further, the orbitofrontal cortex is not only a region where Aβ pathology accumulates early but is also a highly plastic late-developing region, typically affected in aging (**Fjell et al., 2014**; **Pichet Binette et al., 2020**). This might in part explain why the uncinate fasciculus is preferentially affected in preclinical sporadic AD compared to the younger mutation carriers of ADAD.

The direct investigation of WM fiber bundles and their microstructure was possible due to recent advances in diffusion imaging modeling, tractography, bundle extraction, and tractometry quantification. However, there are several limitations to these techniques and to our study. First, there are no common standards (yet) to extract predefined bundles from tractograms, and bundles with high curvature are more challenging to extract. To mitigate this challenge, we mostly relied on algorithms that use priors to help generate fuller bundles. We also used automated algorithms to increase reproducibility and performed rigorous visual inspection to make sure all algorithms yielded comparable bundles. The diffusion sequence, similar in both cohorts, relied on only one b-value, and future acquisitions with multiple b-values could further improve capturing fine-grained changes (**Pines et al., 2020**). We should also note that the PREVENT-AD cohort does not present highly elevated levels of tau, hence the deliberate choice of focusing on the proportion of participants with the highest levels rather than applying a definite cut-off. The sample size might not be huge, but we replicate all main findings in our two groups of interest. Both cohorts are also followed over time on

cognition and imaging, so future longitudinal studies can help clarify the sequence of events between pathology and WM changes in the preclinical and early symptomatic stages.

Overall, we used state-of-the-art analytical techniques to study associations between WM microstructure and Aβ- and tau-PET in key bundles affected in AD in the PREVENT-AD cohort of cognitively normal older adults whose strong family history of AD suggests an increased risk of subsequent dementia (**Cupples et al., 2004**; **Devi et al., 2000**) and in presymptomatic mutation carriers from the DIAN cohort. We highlighted the vulnerability of WM bundles to early presence of Aβ and tau proteins. More generally, the topography of our results aligns with the concept of retrogenesis, postulating that late-myelinated fibers, from temporal and neocortical regions, are affected first in the disease course and less resistant to neurodegeneration (**Alves et al., 2015**; **Bartzokis, 2004**; **Bartzokis, 2011**). As more studies highlight that WM changes might precede changes in GM (**Caso et al., 2016**; **Sachdev et al., 2013**), further investigations of WM microstructure in the early stages of AD will help understand better the complex pathogenesis of the disease.

Materials and methods

Participants

PREVENT-AD

We studied cognitively unimpaired participants at risk of sporadic AD dementia from the PREVENT-AD study. PREVENT-AD is a longitudinal study that started in 2012 (**Breitner et al., 2016**) and enrolled 386 participants. Inclusion criteria were as follows: (1) having intact cognition; (2) having a parent or two siblings diagnosed with AD-like dementia, and therefore being at increased risk of sporadic AD; (3) being above 60 years of age, or between 55 and 59 if fewer than 15 years from their affected family member's age at symptom onset; and (4) being free of major neurological and psychiatric diseases. Overall participants presented low vascular risk factors and about 28% took anti-hypertensive drugs (**Köbe et al., 2020**). Intact cognition was based on the Montreal Cognitive Assessment, a Clinical Dementia Rating of 0, and a standardized neuropsychological evaluation using the Repeatable Battery for the Assessment of Neuropsychological Status (**Randolph et al., 1998**). The cognitive status of individuals with questionable neuropsychological status was reviewed in consensus meetings of neuropsychologists (including SV) and/or psychiatrists. Annual visits include neuropsychological testing and an MRI session. Since 2017, Aβ and tau PET scans were integrated to the study protocol for interested participants. The present study includes participants who had structural and diffusion-weighted MRI and who underwent PET, for a total of 126 participants. All participants included in the current study were cognitively normal at the time they underwent neuroimaging. All underwent diffusion MRI an average of 1.1 ± 0.8 years prior to PET imaging (one completed MRI 5 years prior to PET, but results were unchanged when this participant was removed from analyses).

DIAN

The DIAN study group enrolls individuals over 18 years old with a family history of ADAD. We had access to the DIAN data-freeze 11 of November 2016, from which we selected participants who were cognitively normal as evidenced by Clinical Dementia Rating (**Morris, 1993**) of 0, and who underwent both Aβ-PET and diffusion MRI. Out of the 302 participants with a baseline visit with imaging, 201 underwent diffusion MRI with 64 directions (we excluded 12 participants who only had diffusion MRI with 32 directions), and from those, 177 had Aβ-PET and all demographics available. The final sample thus comprised 81 mutation carriers (49 PSEN1 mutation carriers, 15 PSEN2 mutation carriers, and 17 APP mutation carriers) and 96 mutation non-carriers. Less than 1% of mutation carriers and 14% of non-carriers were categorized as having hypertension.

Image acquisition

Magnetic resonance imaging

PREVENT-AD is a single-site study. All MRI images were acquired on a Magnetom Tim Trio 3 Tesla (Siemens) scanner at the Douglas Mental Health University Institute prior to PET imaging. Structural scans were acquired yearly, and thus we selected the closest scan prior to PET (average time between PET and structural MRI: 8 ± 4 months). Diffusion-weighted MRI was not acquired every

year, and again the diffusion scan closest to PET was chosen for analysis (average time between PET and diffusion-weighted MRI: 1.1 ± 0.8 years). DIAN is a multisite study, and the imaging protocols (MRI and PET) were unified across the different study sites. MRI was also acquired on Siemens 3T scanners (BioGraph mMR PET-MR or Trio). All imaging data were selected from the baseline visit of every participant.

In both studies, the T1-weighted structural image was acquired using a MPRAGE sequence similar to the Alzheimer Disease Neuroimaging Initiative protocol (TR = 2300 ms; TE = 2.98 ms; FA = 9°; FoV = 256 mm; slice thickness = 1 mm; 160–170 slices). In both cohorts, diffusion-weighted MRI consisted of one b0 image and 64 diffusion-weighted volumes acquired with a b-value of 1000 s/mm^2. The PREVENT-AD sequence parameters were the following: TR = 9300 ms, TE = 92 ms, FoV = 130 mm, 2 mm voxels. The DIAN sequence parameters were the following: TR = 11500 ms, T = 87 ms, 2.5 mm voxels.

Positron emission tomography

In PREVENT-AD, PET was performed using [^{18}F]NAV4694 to assess Aβ burden and flortaucipir ([^{18}F]AV1451) to assess tau deposition. PET scanning took place at the McConnell Brain Imaging Centre at the Montreal Neurological Institute using a brain-dedicated PET Siemens/CT high-resolution research tomograph (HRRT) on two consecutive days. Aβ scans were acquired 40–70 min post-injection (≈6 mCi) and tau scans 80–100 min post-injection (≈10 mCi). All scans were completed between March 2017 and April 2019.

In DIAN, PET was performed using Pittsburgh compound B ([^{11}C]PIB) to assess Aβ deposition either with full dynamic or an acquisition 40–70 min post-injection (≈15 mCi).

Positron emission tomography processing

PREVENT-AD PET scans were processed using a standard pipeline (see https://github.com/villeneu-velab/vlpp for more details; ***Bedetti, 2019***). Briefly, Aβ- and *tau*-PET images were realigned, averaged, and registered to the T1-weighted scan of each participant, which had been segmented with the Desikan–Killiany atlas using FreeSurfer version 5.3 (***Desikan et al., 2006***). The same structural scan was used in the diffusion and the PET pipelines. PET images were then masked to remove the scalp and cerebrospinal fluid to reduce contamination by non-grey and non-WM voxels. Standardized uptake value ratios (SUVR) images were obtained using the whole cerebellum as reference region for Aβ-PET (***Jagust et al., 2015***) and the inferior cerebellar GM for tau-PET (***Baker et al., 2017***). A global Aβ burden was calculated from the average bilateral SUVR of medial and lateral frontal, parietal, and temporal regions, and as described previously, participants with an average global Aβ > 1.37 SUVR were considered Aβ-positive (***McSweeney et al., 2020***). For tau, we focused on the average bilateral tau uptake in the entorhinal cortex as it is among the earliest cortical region to be affected over the course of AD (***Braak and Braak, 1991***; ***Maass et al., 2017***). Given that there is no consensus yet as to how to define tau-positivity (***Villemagne et al., 2021***) and that the presence of Aβ is needed to facilitate the accumulation of tau (***Jack et al., 2019***), we considered the same proportion of Aβ-positive and tau-positive participants in PREVENT-AD. As such, participants in the top 20% of tau uptake in the entorhinal cortex were considered tau-positive. In the tau-positive group, 60% of participants were also amyloid-positive.

DIAN PET scans were processed by the DIAN image processing core and made available after extensive quality control. Briefly, PET images were registered to the structural image that had been processed with FreeSurfer 5.3. PET images were converted to regional SUVR using the cerebellar GM as reference region (***Su et al., 2013***), and a regional spread function-based approach for partial volume correction was applied (***Su et al., 2015***). A global Aβ burden was calculated from averaging the SUVR of four cortical regions (prefrontal, gyrus rectus, lateral temporal, and precuneus) typically used in the DIAN study group (***Morris et al., 2010***). Participants with a global Aβ SUVR above 1.42 were considered Aβ-positive, as established previously (***Mishra et al., 2018***; ***Schultz et al., 2020***; ***Su et al., 2019***).

Diffusion MRI processing

An overview of the processing steps is displayed in ***Figure 1***.

Preprocessing steps

The diffusion-weighted images were processed using the TractoFlow Atlas-Based Segmentation (TractoFlow-ABS) pipeline. TractoFlow-ABS is an extension of the recent TractoFlow pipeline (**Theaud et al., 2020a**) publicly available for academic research purposes (https://github.com/scilus/tractoflow-ABS; **Theaud, 2020b**) that uses Nextflow (**Di Tommaso et al., 2017**) and Singularity (**Kurtzer et al., 2017**) to ensure efficient and reproducible diffusion processing. All major processing steps are performed through this pipeline, from preprocessing of the structural and diffusion images to tractography. The pipeline computes typical DTI maps, fODF, and a whole-brain tractogram. The pipeline calls different functions from various neuroimaging software, namely FSL (**Jenkinson et al., 2012**), MRtrix3 (**Tournier et al., 2019**), ANTs (**Avants et al., 2011**), and DIPY (**Garyfallidis et al., 2014**). For a detailed description of the different steps, see **Theaud et al., 2020a**.

Diffusion measures

After the preprocessing steps, different diffusion measures can be generated as part of TractoFlow-ABS. The following DTI measures were computed using DIPY: FA, MD, RD, and AD. Along with typical DTI modeling, fODFs were also computed using constrained spherical deconvolution (**Descoteaux et al., 2007**; **Tournier et al., 2007**) and the fiber response function from the group average.

We also generated FW-corrected DTI measures, which were the main diffusion measures of interest in this study. FW correction has been proposed as a way to remove the contamination of water from the tissue properties by modeling the isotropic diffusion of the FW component (**Pasternak et al., 2009**). FW modeling was performed using the accelerated microstructure imaging via convex optimization (**Daducci et al., 2015**) to calculate FW index and FW-corrected measures, namely FA_T, MD_T, AD_T, and RD_T. Processing was done using the freely available FreeWater pipeline (https://github.com/scilus/freewater_flow, **Bore, 2020**). Removing the contribution of FW is thought to better represent the tissue microstructure (hence the subscript T for tissue) and might be more sensitive than the non-corrected measures (**Albi et al., 2017**; **Chad et al., 2018**; **Pasternak et al., 2012**).

Tractography

The last step of the pipeline is tractography. This is where TractoFlow and TractoFlow-ABS differ. The former uses a more sophisticated algorithm, particle filtering tractography, that takes into account anatomical information to reduce tractography biases (**Girard et al., 2014**). Such an algorithm requires probabilistic maps of GM, WM and cerebrospinal fluid to add additional constraints for tracking. However, with aging, probabilistic maps in 'bottleneck' areas of WM fibers, for example, where the uncinate fasciculus bends, show poorer distinction between GM and WM voxels. Furthermore, increasing WM hyperintensities and general atrophy with aging also complicates the use of more advanced algorithms. As a result, the performance of particle filtering tractography was affected and failed to generate bundles suitable for analysis. Instead, as implemented in TractoFlow-ABS, we opted for local tracking with a probabilistic algorithm to reconstruct whole-brain tractograms. The inputs for tracking were the fODF image for directions and a WM mask for seeding. The mask was computed by joining the WM and the subcortical masks from the structural image that had been segmented with the Desikan–Killiany atlas in FreeSurfer version 5.3 (**Desikan et al., 2006**). For tracking, seeding was initiated in voxels from the WM mask with 10 seeds per voxel. The tractograms had between 2 and 3 million streamlines.

White matter bundles extraction

From the tractogram, we extracted different bundles of interest. We focused on bundles connecting the main brain region where Aβ and tau accumulate in the early phase of AD, namely the uncinate fasciculus, the anterior cingulum, and the posterior cingulum. To extract the uncinate fasciculus and the anterior cingulum, we used RecoBundlesX (**Rheault, 2020**), an automated algorithm to segment the tractograms into different bundles. This algorithm is an improved and more stable version of RecoBundles (**Garyfallidis et al., 2018**). Briefly, the method is based on shape priors to detect similarity in streamlines. Taking the whole-brain tractogram and templates from the bundles of interest as inputs, RecoBundlesX extracts bundles based on the shape of the streamlines from the templates.

The difference between RecoBundles and RecoBundlesX resides in that the latter can take multiple templates as inputs and multiple parameters, which refines which streamlines are included or excluded from the final bundle. RecoBundlesX is typically run 80 times and the output is the conjunction of the multiple runs, yielding more robust bundles. RecoBundlesX does not include templates for the posterior cingulum, and thus we used TractQuerier (***Wassermann et al., 2016***) for this bundle. This method works with customizable queries to extract bundles based on anatomical definitions. Using inclusion and exclusion regions of interest based on the FreeSurfer parcellation, we implemented a query specifically for the posterior cingulum, as used in another recent study (***Roy et al., 2020***), which can be found in Supplementary Material.

After extracting all bundles, there were inspected visually in MI-Brain (https://www.imeka.ca/fr/mi-brain/) to make sure the shape, location, and size were adequate.

Bundle-specific quantification with tractometry

The last step required to put together the different WM measures and bundles of interest was tractometry (***Cousineau et al., 2017***). Tractometry is a way to extract the measures of interest specifically in each bundle. It takes as input the maps of all microstructure measures and the bundles in which we want to extract them. In our case, we extracted the average tissue measures (FA_T, MD_T, RD_T, AD_T, and FW index) for each bundle (uncinate fasciculus, cingulum, posterior cingulum). For complementary analyses, we also extracted typical tensor measures (average FA, MD, RD, and AD) in each bundle. The overall approach, done entirely in native space, has the advantage of generating bundles specific to each individual.

Statistical analysis

Partial correlations were performed to evaluate the relationships between Aβ- or tau-PET and the different microstructure measures in each bundle, controlling for age, sex, and bundle volume. In primary analyses, the diffusion measures investigated as independent variables were FA_T, MD_T, RD_T, AD_T, and FW index. Analyses were performed separately in left and right bundles for Aβ and tau. The dependent variables were global cortical Aβ and entorhinal tau SUVR. We display bivariate associations between diffusion and PET measures to show the raw data, but we based the results on the partial correlation coefficient of the diffusion measure, controlling for age, sex, and bundle volume (divided by total intracranial volume). Models were first performed at the whole-group level and then specifically in the Aβ-positive or tau-positive groups versus the Aβ- or tau-negative groups. We reasoned that the participants harboring pathology (and thus being in the preclinical stage of the disease) would be the most likely to show WM degeneration. We repeated the analyses including either APOE ε4 status or handedness as a covariate in the models. Since the results were mainly unchanged, these data are not presented. In the bundles where associations were found between pathology and microstructure, we further controlled for GM volume (divided by total intracranial volume) of cortical regions connected by the given bundle to evaluate whether associations were also influenced by atrophy. For the uncinate fasciculus, GM regions of interest were the medial orbitofrontal cortex and the parahippocampal gyrus; for the cingulum, regions were the anterior and posterior cingulate; and for the posterior cingulum, regions were precuneus and parahippocampal gyrus. We also performed similar analyses with the typical tensor measures (FA, MD, AD, and RD) to evaluate whether the FW-corrected measures were more sensitive. Associations with a p-value < 0.05 were considered significant. Analyses were conducted using SPSS version 27 (IBM, NY, USA) and R version 3.6.3 (***R Development Core Team, 2020***).

Acknowledgements

We wish to acknowledge the staff of PREVENT-AD as well as of the Brain Imaging Centre of the Douglas Mental Health University Institute and of the PET unit of the McConnell Brain Imaging Centre of the Montreal Neurological Institute, and members of the SCIL lab. A full listing of members of the PREVENT-AD Research Group can be found at https://preventad.loris.ca/acknowledgements/acknowledgements.php?date=[2020-06-30]. We would also like to acknowledge the participants of the PREVENT-AD cohort for dedicating their time and energy to helping us collect these data. Thank you to the Neuroinformatics Chair of the Université de Sherbrooke for supporting neuroscience research. Data collection and sharing for this project was supported by The Dominantly Inherited

Alzheimer's Network (DIAN, UF1AG032438) funded by the National Institute on Aging (NIA), the German Center for Neurodegenerative Diseases (DZNE), Raul Carrea Institute for Neurological Research (FLENI), partial support by the Research and Development Grants for Dementia from Japan Agency for Medical Research and Development, AMED, and the Korea Health Technology R&D Project through the Korea Health Industry Development Institute (KHIDI). This manuscript has been reviewed by DIAN Study investigators for scientific content and consistency of data interpretation with previous DIAN Study publications. We acknowledge the altruism of the participants and their families and contributions of the DIAN research and support staff at each of the participating sites for their contributions to this study.

Additional information

Competing interests

Johannes Levin: reports speaker fees from Bayer Vital and Roche, consulting fees from Axon Neuroscience, author fees from Thieme medical publishers and W. Kohlhammer GmbH medical publishers, non-financial support from Abbvie and compensation for duty as part-time CMO from MODAG, outside the submitted work. Maxime Descoteaux: is the co-founder of Imeka Solution Inc. The other authors declare that no competing interests exist.

Funding

Funder	Grant reference number	Author
Canadian Institutes of Health Research	PJT-162091	Sylvia Villeneuve
Canadian Institutes of Health Research	PJT-148963	Sylvia Villeneuve
Jean-Louis Lévesque Foundation		Judes Poirier
Douglas Foundation		John CS Breitner
Canada Foundation for Innovation		Sylvia Villeneuve
NIA	UF1AG032438	DIAN Study Group

The funders had no role in study design, data collection and interpretation, or the decision to submit the work for publication.

Author contributions

Alexa Pichet Binette, Conceptualization, Formal analysis, Visualization, Writing - original draft; Guillaume Theaud, Software, Methodology, Writing - review and editing; François Rheault, Software, Methodology; Maggie Roy, Conceptualization, Writing - review and editing; D Louis Collins, Funding acquisition, Writing - review and editing; Johannes Levin, Hiroshi Mori, Jae Hong Lee, Peter Schofield, Resources, Project administration; Martin Rhys Farlow, Colin L Masters, Resources, Funding acquisition, Project administration, Writing - review and editing; Jasmeer P Chhatwal, John Morris, Judes Poirier, Maxime Descoteaux, Conceptualization, Resources, Software, Supervision, Funding acquisition, Methodology, Project administration, Writing - review and editing; Tammie Benzinger, John CS Breitner, Conceptualization, Resources, Data curation, Software, Supervision, Funding acquisition, Methodology, Project administration, Writing - review and editing; Randall Bateman, Julie Gonneaud, Conceptualization, Resources, Data curation, Supervision, Funding acquisition, Project administration, Writing - review and editing; Sylvia Villeneuve, Conceptualization, Supervision, Funding acquisition, Project administration, Writing - review and editing; DIAN Study Group, PREVENT-AD Research Group, Resources

Author ORCIDs

Alexa Pichet Binette https://orcid.org/0000-0001-5218-3337
D Louis Collins http://orcid.org/0000-0002-8432-7021

Ethics

Human subjects: The study was approved by the ethics committee of the Faculty of Medicine of McGill University and of the Douglas Mental Health University Institute. Informed consent was obtained from all PREVENT-AD and DIAN participants prior to enrolling in the respective studies. We had access to the DIAN data with approval from DIAN leaders (data request DIAN-D1624).

Decision letter and Author response

Decision letter https://doi.org/10.7554/eLife.62929.sa1
Author response https://doi.org/10.7554/eLife.62929.sa2

Additional files

Supplementary files

- Transparent reporting form

Data availability

All raw imaging data from PREVENT-AD is openly available to researchers on the data repository https://registeredpreventad.loris.ca/.

The following dataset was generated:

Author(s)	Year	Dataset title	Dataset URL	Database and Identifier
Madjar C	2021	PREVENT-AD	https://doi.org/10.5281/zenodo.4298795	Zenodo, 10.5281/zenodo.4298795

References

Agosta F, Pievani M, Sala S, Geroldi C, Galluzzi S, Frisoni GB, Filippi M. 2011. White matter damage in alzheimer disease and its relationship to gray matter atrophy. *Radiology* **258**:853–863. DOI: https://doi.org/10.1148/radiol.10101284, PMID: 21177393

Ahmed Z, Cooper J, Murray TK, Garn K, McNaughton E, Clarke H, Parhizkar S, Ward MA, Cavallini A, Jackson S, Bose S, Clavaguera F, Tolnay M, Lavenir I, Goedert M, Hutton ML, O'Neill MJ. 2014. A novel in vivo model of tau propagation with rapid and progressive neurofibrillary tangle pathology: the pattern of spread is determined by connectivity, not proximity. *Acta Neuropathologica* **127**:667–683. DOI: https://doi.org/10.1007/s00401-014-1254-6, PMID: 24531916

Albi A, Pasternak O, Minati L, Marizzoni M, Bartrés-Faz D, Bargalló N, Bosch B, Rossini PM, Marra C, Müller B, Fiedler U, Wiltfang J, Roccatagliata L, Picco A, Nobili FM, Blin O, Sein J, Ranjeva JP, Didic M, Bombois S, et al. 2017. Free water elimination improves test-retest reproducibility of diffusion tensor imaging indices in the brain: a longitudinal multisite study of healthy elderly subjects. *Human Brain Mapping* **38**:12–26. DOI: https://doi.org/10.1002/hbm.23350, PMID: 27519630

Alves GS, Oertel Knöchel V, Knöchel C, Carvalho AF, Pantel J, Engelhardt E, Laks J. 2015. Integrating retrogenesis theory to Alzheimer's disease pathology: insight from DTI-TBSS investigation of the white matter microstructural integrity. *BioMed Research International* **2015**:1–11. DOI: https://doi.org/10.1155/2015/291658

Amlien IK, Fjell AM. 2014. Diffusion tensor imaging of white matter degeneration in Alzheimer's disease and mild cognitive impairment. *Neuroscience* **276**:206–215. DOI: https://doi.org/10.1016/j.neuroscience.2014.02.017, PMID: 24583036

Araque Caballero MÁ, Suárez-Calvet M, Duering M, Franzmeier N, Benzinger T, Fagan AM, Bateman RJ, Jack CR, Levin J, Dichgans M, Jucker M, Karch C, Masters CL, Morris JC, Weiner M, Rossor M, Fox NC, Lee JH, Salloway S, Danek A, et al. 2018. White matter diffusion alterations precede symptom onset in autosomal dominant alzheimer's disease. *Brain* **141**:3065–3080. DOI: https://doi.org/10.1093/brain/awy229, PMID: 30239611

Avants BB, Tustison NJ, Song G, Cook PA, Klein A, Gee JC. 2011. A reproducible evaluation of ANTs similarity metric performance in brain image registration. *NeuroImage* **54**:2033–2044. DOI: https://doi.org/10.1016/j.neuroimage.2010.09.025, PMID: 20851191

Badea A, Kane L, Anderson RJ, Qi Y, Foster M, Cofer GP, Medvitz N, Buckley AF, Badea AK, Wetsel WC, Colton CA. 2016. The fornix provides multiple biomarkers to characterize circuit disruption in a mouse model of

alzheimer's disease. *NeuroImage* **142**:498–511. DOI: https://doi.org/10.1016/j.neuroimage.2016.08.014, PMID: 27521741

Baker SL, Maass A, Jagust WJ. 2017. Considerations and code for partial volume correcting [^{18}F]-AV-1451 tau PET data. *Data in Brief* **15**:648–657. DOI: https://doi.org/10.1016/j.dib.2017.10.024, PMID: 29124088

Bartzokis G. 2004. Age-related myelin breakdown: a developmental model of cognitive decline and Alzheimer's disease. *Neurobiology of Aging* **25**:5–18. DOI: https://doi.org/10.1016/j.neurobiolaging.2003.03.001, PMID: 14675724

Bartzokis G. 2011. Alzheimer's disease as homeostatic responses to age-related myelin breakdown. *Neurobiology of Aging* **32**:1341–1371. DOI: https://doi.org/10.1016/j.neurobiolaging.2009.08.007, PMID: 19775776

Bateman RJ, Xiong C, Benzinger TLS, Fagan AM, Goate A, Fox NC, Marcus DS, Cairns NJ, Xie X, Blazey TM, Holtzman DM, Santacruz A, Buckles V, Oliver A, Moulder K, Aisen PS, Ghetti B, Klunk WE, McDade E, Martins RN, et al. 2012. Clinical and biomarker changes in dominantly inherited Alzheimer's Disease. *New England Journal of Medicine* **367**:795–804. DOI: https://doi.org/10.1056/NEJMoa1202753

Bedetti C. 2019. Villeneuve Laboratory PET Pipeline (VLPP). *GitHib*. https://github.com/villeneuvelab/vlpp

Berron D, van Westen D, Ossenkoppele R, Strandberg O, Hansson O. 2020. Medial temporal lobe connectivity and its associations with cognition in early Alzheimer's disease. *Brain* **143**:1233–1248. DOI: https://doi.org/10.1093/brain/awaa068, PMID: 32252068

Bore A. 2020. FreeWater and FW corrected DTI metrics pipeline. *GitHub*. https://github.com/scilus/freewater_flow

Braak H, Thal DR, Ghebremedhin E, Del Tredici K. 2011. Stages of the pathologic process in alzheimer disease: age categories from 1 to 100 years. *Journal of Neuropathology & Experimental Neurology* **70**:960–969. DOI: https://doi.org/10.1097/NEN.0b013e318232a379, PMID: 22002422

Braak H, Braak E. 1991. Neuropathological stageing of Alzheimer-related changes. *Acta Neuropathologica* **82**:239–259. DOI: https://doi.org/10.1007/BF00308809, PMID: 1759558

Breitner JCS, Poirier J, Etienne PE, Leoutsakos JM. 2016. Rationale and structure for a new center for studies on prevention of Alzheimer's Disease (StoP-AD). *Journal of Prevention of Alzheimer's Disease* **3**:236–242. DOI: https://doi.org/10.14283/jpad.2016.121

Bubb EJ, Metzler-Baddeley C, Aggleton JP. 2018. The cingulum bundle: anatomy, function, and dysfunction. *Neuroscience & Biobehavioral Reviews* **92**:104–127. DOI: https://doi.org/10.1016/j.neubiorev.2018.05.008, PMID: 29753752

Caso F, Agosta F, Filippi M. 2016. Insights into white matter damage in Alzheimer's Disease: From Postmortem to in vivo Diffusion Tensor MRI Studies. *Neurodegenerative Diseases* **16**:26–33. DOI: https://doi.org/10.1159/000441422, PMID: 26618812

Chad JA, Pasternak O, Salat DH, Chen JJ. 2018. Re-examining age-related differences in white matter microstructure with free-water corrected diffusion tensor imaging. *Neurobiology of Aging* **71**:161–170. DOI: https://doi.org/10.1016/j.neurobiolaging.2018.07.018, PMID: 30145396

Cousineau M, Jodoin PM, Morency FC, Rozanski V, Grand'Maison M, Bedell BJ, Descoteaux M. 2017. A test-retest study on parkinson's PPMI dataset yields statistically significant white matter fascicles. *NeuroImage: Clinical* **16**:222–233. DOI: https://doi.org/10.1016/j.nicl.2017.07.020, PMID: 28794981

Cupples LA, Farrer LA, Sadovnick AD, Relkin N, Whitehouse P, Green RC. 2004. Estimating risk curves for first-degree relatives of patients with Alzheimer's disease: the REVEAL study. *Genetics in Medicine* **6**:192–196. DOI: https://doi.org/10.1097/01.GIM.0000132679.92238.58, PMID: 15266206

Daducci A, Canales-Rodríguez EJ, Zhang H, Dyrby TB, Alexander DC, Thiran JP. 2015. Accelerated microstructure imaging via convex optimization (AMICO) from diffusion MRI data. *NeuroImage* **105**:32–44. DOI: https://doi.org/10.1016/j.neuroimage.2014.10.026, PMID: 25462697

Descoteaux M, Angelino E, Fitzgibbons S, Deriche R. 2007. Regularized, fast, and robust analytical Q-ball imaging. *Magnetic Resonance in Medicine* **58**:497–510. DOI: https://doi.org/10.1002/mrm.21277, PMID: 17763358

Desikan RS, Ségonne F, Fischl B, Quinn BT, Dickerson BC, Blacker D, Buckner RL, Dale AM, Maguire RP, Hyman BT, Albert MS, Killiany RJ. 2006. An automated labeling system for subdividing the human cerebral cortex on MRI scans into gyral based regions of interest. *NeuroImage* **31**:968–980. DOI: https://doi.org/10.1016/j.neuroimage.2006.01.021, PMID: 16530430

Devi G, Ottman R, Tang MX, Marder K, Stern Y, Mayeux R. 2000. Familial aggregation of alzheimer disease among whites, african americans, and Caribbean hispanics in northern Manhattan. *Archives of Neurology* **57**:72–77. DOI: https://doi.org/10.1001/archneur.57.1.72, PMID: 10634451

Di Tommaso P, Chatzou M, Floden EW, Barja PP, Palumbo E, Notredame C. 2017. Nextflow enables reproducible computational workflows. *Nature Biotechnology* **35**:316–319. DOI: https://doi.org/10.1038/nbt.3820, PMID: 28398311

Dong JW, Jelescu IO, Ades-Aron B, Novikov DS, Friedman K, Babb JS, Osorio RS, Galvin JE, Shepherd TM, Fieremans E. 2020. Diffusion MRI biomarkers of white matter microstructure vary nonmonotonically with increasing cerebral amyloid deposition. *Neurobiology of Aging* **89**:118–128. DOI: https://doi.org/10.1016/j.neurobiolaging.2020.01.009, PMID: 32111392

Duyckaerts C, Delatour B, Potier MC. 2009. Classification and basic pathology of alzheimer disease. *Acta Neuropathologica* **118**:5–36. DOI: https://doi.org/10.1007/s00401-009-0532-1, PMID: 19381658

Dyrby TB, Lundell H, Burke MW, Reislev NL, Paulson OB, Ptito M, Siebner HR. 2014. Interpolation of diffusion weighted imaging datasets. *NeuroImage* **103**:202–213. DOI: https://doi.org/10.1016/j.neuroimage.2014.09.005, PMID: 25219332

Finsterwalder S, Vlegels N, Gesierich B, Araque Caballero MÁ, Weaver NA, Franzmeier N, Georgakis MK, Konieczny MJ, Koek HL, Karch CM, Graff-Radford NR, Salloway S, Oh H, Allegri RF, Chhatwal JP, Jessen F, Düzel E, Dobisch L, Metzger C, Peters O, et al. 2020. Small vessel disease more than Alzheimer's disease determines diffusion MRI alterations in memory clinic patients. *Alzheimer's & Dementia* **16**:1504–1514. DOI: https://doi.org/10.1002/alz.12150, PMID: 32808747

Fjell AM, McEvoy L, Holland D, Dale AM, Walhovd KB, Alzheimer's Disease Neuroimaging Initiative. 2014. What is normal in normal aging? effects of aging, amyloid and Alzheimer's disease on the cerebral cortex and the hippocampus. *Progress in Neurobiology* **117**:20–40. DOI: https://doi.org/10.1016/j.pneurobio.2014.02.004, PMID: 24548606

Fortea J, Sala-Llonch R, Bartrés-Faz D, Bosch B, Lladó A, Bargalló N, Molinuevo JL, Sánchez-Valle R. 2010. Increased cortical thickness and caudate volume precede atrophy in PSEN1 mutation carriers. *Journal of Alzheimer's Disease* **22**:909–922. DOI: https://doi.org/10.3233/JAD-2010-100678, PMID: 20858974

Franzmeier N, Rubinski A, Neitzel J, Kim Y, Damm A, Na DL, Kim HJ, Lyoo CH, Cho H, Finsterwalder S, Duering M, Seo SW, Ewers M, Alzheimer's Disease Neuroimaging Initiative. 2019. Functional connectivity associated with tau levels in ageing, alzheimer's, and small vessel disease. *Brain* **142**:1093–1107. DOI: https://doi.org/10.1093/brain/awz026, PMID: 30770704

Franzmeier N, Neitzel J, Rubinski A, Smith R, Strandberg O, Ossenkoppele R, Hansson O, Ewers M, Alzheimer's Disease Neuroimaging Initiative (ADNI). 2020. Functional brain architecture is associated with the rate of tau accumulation in Alzheimer's disease. *Nature Communications* **11**:347. DOI: https://doi.org/10.1038/s41467-019-14159-1, PMID: 31953405

Garyfallidis E, Brett M, Amirbekian B, Rokem A, van der Walt S, Descoteaux M, Nimmo-Smith I, Dipy Contributors. 2014. Dipy, a library for the analysis of diffusion MRI data. *Frontiers in Neuroinformatics* **8**:8. DOI: https://doi.org/10.3389/fninf.2014.00008, PMID: 24600385

Garyfallidis E, Côté MA, Rheault F, Sidhu J, Hau J, Petit L, Fortin D, Cunanne S, Descoteaux M. 2018. Recognition of white matter bundles using local and global streamline-based registration and clustering. *NeuroImage* **170**:283–295. DOI: https://doi.org/10.1016/j.neuroimage.2017.07.015, PMID: 28712994

Girard G, Whittingstall K, Deriche R, Descoteaux M. 2014. Towards quantitative connectivity analysis: reducing tractography biases. *NeuroImage* **98**:266–278. DOI: https://doi.org/10.1016/j.neuroimage.2014.04.074, PMID: 24816531

Gordon BA, Blazey TM, Christensen J, Dincer A, Flores S, Keefe S, Chen C, Su Y, McDade EM, Wang G, Li Y, Hassenstab J, Aschenbrenner A, Hornbeck R, Jack CR, Ances BM, Berman SB, Brosch JR, Galasko D, Gauthier S, et al. 2019. Tau PET in autosomal dominant Alzheimer's disease: relationship with cognition, dementia and other biomarkers. *Brain* **142**:1063–1076. DOI: https://doi.org/10.1093/brain/awz019, PMID: 30753379

Harrison JR, Bhatia S, Tan ZX, Mirza-Davies A, Benkert H, Tax CMW, Jones DK. 2020. Imaging alzheimer's genetic risk using diffusion MRI: A systematic review. *NeuroImage: Clinical* **27**:102359. DOI: https://doi.org/10.1016/j.nicl.2020.102359, PMID: 32758801

Iturria-Medina Y, Sotero RC, Toussaint PJ, Mateos-Pérez JM, Evans AC, Alzheimer's Disease Neuroimaging Initiative. 2016. Early role of vascular dysregulation on late-onset alzheimer's disease based on multifactorial data-driven analysis. *Nature Communications* **7**:11934. DOI: https://doi.org/10.1038/ncomms11934, PMID: 27327500

Jack CR, Knopman DS, Jagust WJ, Petersen RC, Weiner MW, Aisen PS, Shaw LM, Vemuri P, Wiste HJ, Weigand SD, Lesnick TG, Pankratz VS, Donohue MC, Trojanowski JQ. 2013. Tracking pathophysiological processes in Alzheimer's disease: an updated hypothetical model of dynamic biomarkers. *The Lancet Neurology* **12**:207–216. DOI: https://doi.org/10.1016/S1474-4422(12)70291-0, PMID: 23332364

Jack CR, Wiste HJ, Botha H, Weigand SD, Therneau TM, Knopman DS, Graff-Radford J, Jones DT, Ferman TJ, Boeve BF, Kantarci K, Lowe VJ, Vemuri P, Mielke MM, Fields JA, Machulda MM, Schwarz CG, Senjem ML, Gunter JL, Petersen RC. 2019. The bivariate distribution of amyloid-β and tau: relationship with established neurocognitive clinical syndromes. *Brain* **142**:3230–3242. DOI: https://doi.org/10.1093/brain/awz268, PMID: 31501889

Jacobs HIL, Hedden T, Schultz AP, Sepulcre J, Perea RD, Amariglio RE, Papp KV, Rentz DM, Sperling RA, Johnson KA. 2018. Structural tract alterations predict downstream tau accumulation in amyloid-positive older individuals. *Nature Neuroscience* **21**:424–431. DOI: https://doi.org/10.1038/s41593-018-0070-z, PMID: 29403032

Jagust WJ, Landau SM, Koeppe RA, Reiman EM, Chen K, Mathis CA, Price JC, Foster NL, Wang AY. 2015. The alzheimer's Disease Neuroimaging Initiative 2 PET Core: 2015. *Alzheimer's & Dementia* **11**:757–771. DOI: https://doi.org/10.1016/j.jalz.2015.05.001, PMID: 26194311

Jansen WJ, Ossenkoppele R, Knol DL, Tijms BM, Scheltens P, Verhey FR, Visser PJ, Aalten P, Aarsland D, Alcolea D, Alexander M, Almdahl IS, Arnold SE, Baldeiras I, Barthel H, van Berckel BN, Bibeau K, Blennow K, Brooks DJ, van Buchem MA, et al. 2015. Prevalence of cerebral amyloid pathology in persons without dementia: a meta-analysis. *Jama* **313**:1924–1938. DOI: https://doi.org/10.1001/jama.2015.4668, PMID: 25988462

Jenkinson M, Beckmann CF, Behrens TE, Woolrich MW, Smith SM. 2012. FSL. *NeuroImage* **62**:782–790. DOI: https://doi.org/10.1016/j.neuroimage.2011.09.015, PMID: 21979382

Johnson KA, Schultz A, Betensky RA, Becker JA, Sepulcre J, Rentz D, Mormino E, Chhatwal J, Amariglio R, Papp K, Marshall G, Albers M, Mauro S, Pepin L, Alverio J, Judge K, Philiossaint M, Shoup T, Yokell D, Dickerson B,

et al. 2016. Tau positron emission tomographic imaging in aging and early alzheimer disease. *Annals of Neurology* **79**:110–119. DOI: https://doi.org/10.1002/ana.24546, PMID: 26505746

Jones DT, Knopman DS, Gunter JL, Graff-Radford J, Vemuri P, Boeve BF, Petersen RC, Weiner MW, Jack CR, Alzheimer's Disease Neuroimaging Initiative. 2016. Cascading network failure across the alzheimer's disease spectrum. *Brain* **139**:547–562. DOI: https://doi.org/10.1093/brain/awv338, PMID: 26586695

Jones DT, Graff-Radford J, Lowe VJ, Wiste HJ, Gunter JL, Senjem ML, Botha H, Kantarci K, Boeve BF, Knopman DS, Petersen RC, Jack CR. 2017. Tau, amyloid, and cascading network failure across the alzheimer's disease spectrum. *Cortex* **97**:143–159. DOI: https://doi.org/10.1016/j.cortex.2017.09.018, PMID: 29102243

Jucker M, Walker LC. 2018. Propagation and spread of pathogenic protein assemblies in neurodegenerative diseases. *Nature Neuroscience* **21**:1341–1349. DOI: https://doi.org/10.1038/s41593-018-0238-6, PMID: 30258241

Kantarci K, Murray ME, Schwarz CG, Reid RI, Przybelski SA, Lesnick T, Zuk SM, Raman MR, Senjem ML, Gunter JL, Boeve BF, Knopman DS, Parisi JE, Petersen RC, Jack CR, Dickson DW. 2017. White-matter integrity on DTI and the pathologic staging of alzheimer's disease. *Neurobiology of Aging* **56**:172–179. DOI: https://doi.org/10.1016/j.neurobiolaging.2017.04.024, PMID: 28552181

Klunk WE, Engler H, Nordberg A, Wang Y, Blomqvist G, Holt DP, Bergström M, Savitcheva I, Huang GF, Estrada S, Ausén B, Debnath ML, Barletta J, Price JC, Sandell J, Lopresti BJ, Wall A, Koivisto P, Antoni G, Mathis CA, et al. 2004. Imaging brain amyloid in Alzheimer's disease with Pittsburgh Compound-B. *Annals of Neurology* **55**:306–319. DOI: https://doi.org/10.1002/ana.20009, PMID: 14991808

Köbe T, Gonneaud J, Pichet Binette A, Meyer PF, McSweeney M, Rosa-Neto P, Breitner JCS, Poirier J, Villeneuve S, Presymptomatic Evaluation of Experimental or Novel Treatments for Alzheimer Disease (PREVENT-AD) Research Group. 2020. Association of vascular risk factors with β-Amyloid peptide and tau burdens in cognitively unimpaired individuals and its interaction with vascular medication use. *JAMA Network Open* **3**:e1920780. DOI: https://doi.org/10.1001/jamanetworkopen.2019.20780, PMID: 32031648

Kurtzer GM, Sochat V, Bauer MW. 2017. Singularity: scientific containers for mobility of compute. *PLOS ONE* **12**:e0177459. DOI: https://doi.org/10.1371/journal.pone.0177459, PMID: 28494014

Maass A, Landau S, Baker SL, Horng A, Lockhart SN, La Joie R, Rabinovici GD, Jagust WJ, Alzheimer's Disease Neuroimaging Initiative. 2017. Comparison of multiple tau-PET measures as biomarkers in aging and Alzheimer's disease. *NeuroImage* **157**:448–463. DOI: https://doi.org/10.1016/j.neuroimage.2017.05.058, PMID: 28587897

Mattsson N, Palmqvist S, Stomrud E, Vogel J, Hansson O. 2019. Staging beta-Amyloid pathology with amyloid positron emission tomography. *JAMA Neurology* **76**:2214. DOI: https://doi.org/10.1001/jamaneurol.2019.2214

McSweeney M, Pichet Binette A, Meyer PF, Gonneaud J, Bedetti C, Ozlen H, Labonté A, Rosa-Neto P, Breitner J, Poirier J, Villeneuve S, PREVENT-AD Research Group. 2020. Intermediate flortaucipir uptake is associated with Aβ-PET and CSF tau in asymptomatic adults. *Neurology* **94**:e1190–e1200. DOI: https://doi.org/10.1212/WNL.0000000000008905, PMID: 32015176

Mishra S, Blazey TM, Holtzman DM, Cruchaga C, Su Y, Morris JC, Benzinger TLS, Gordon BA. 2018. Longitudinal brain imaging in preclinical alzheimer disease: impact of APOE ε4 genotype. *Brain* **141**:1828–1839. DOI: https://doi.org/10.1093/brain/awy103, PMID: 29672664

Mito R, Raffelt D, Dhollander T, Vaughan DN, Tournier JD, Salvado O, Brodtmann A, Rowe CC, Villemagne VL, Connelly A. 2018. Fibre-specific white matter reductions in Alzheimer's disease and mild cognitive impairment. *Brain* **141**:888–902. DOI: https://doi.org/10.1093/brain/awx355, PMID: 29309541

Montal V, Vilaplana E, Alcolea D, Pegueroles J, Pasternak O, González-Ortiz S, Clarimón J, Carmona-Iragui M, Illán-Gala I, Morenas-Rodríguez E, Ribosa-Nogué R, Sala I, Sánchez-Saudinós MB, García-Sebastian M, Villanúa J, Izagirre A, Estanga A, Ecay-Torres M, Iriondo A, Clerigue M, et al. 2018. Cortical microstructural changes along the alzheimer's disease continuum. *Alzheimer's & Dementia* **14**:340–351. DOI: https://doi.org/10.1016/j.jalz.2017.09.013, PMID: 29080407

Mormino EC, Smiljic A, Hayenga AO, Onami SH, Greicius MD, Rabinovici GD, Janabi M, Baker SL, Yen IV, Madison CM, Miller BL, Jagust WJ. 2011. Relationships between β-amyloid and functional connectivity in different components of the default mode network in aging. *Cerebral Cortex* **21**:2399–2407. DOI: https://doi.org/10.1093/cercor/bhr025, PMID: 21383234

Morris JC. 1993. The clinical dementia rating (CDR): current version and scoring rules. *Neurology* **43**:2412–2414. DOI: https://doi.org/10.1212/wnl.43.11.2412-a, PMID: 8232972

Morris JC, Roe CM, Xiong C, Fagan AM, Goate AM, Holtzman DM, Mintun MA. 2010. APOE predicts amyloid-beta but not tau alzheimer pathology in cognitively normal aging. *Annals of Neurology* **67**:122–131. DOI: https://doi.org/10.1002/ana.21843, PMID: 20186853

Morris JC, Aisen PS, Bateman RJ, Benzinger TLS, Cairns NJ, Fagan AM, Ghetti B, Goate AM, Holtzman DM, Klunk WE, McDade E, Marcus DS, Martins RN, Masters CL, Mayeux R, Oliver A, Quaid K, M Ringman J, Rossor MN, Salloway S, et al. 2012. Developing an international network for alzheimer's research: the Dominantly Inherited Alzheimer Network. *Clinical Investigation* **2**:975–984. DOI: https://doi.org/10.4155/cli.12.93

Palop JJ, Mucke L. 2010. Amyloid-beta-induced neuronal dysfunction in Alzheimer's disease: from synapses toward neural networks. *Nature Neuroscience* **13**:812–818. DOI: https://doi.org/10.1038/nn.2583, PMID: 20581818

Pasternak O, Sochen N, Gur Y, Intrator N, Assaf Y. 2009. Free water elimination and mapping from diffusion MRI. *Magnetic Resonance in Medicine* **62**:717–730. DOI: https://doi.org/10.1002/mrm.22055, PMID: 19623619

Pasternak O, Westin CF, Bouix S, Seidman LJ, Goldstein JM, Woo TU, Petryshen TL, Mesholam-Gately RI, McCarley RW, Kikinis R, Shenton ME, Kubicki M. 2012. Excessive extracellular volume reveals a

neurodegenerative pattern in schizophrenia onset. *Journal of Neuroscience* **32**:17365–17372. DOI: https://doi.org/10.1523/JNEUROSCI.2904-12.2012, PMID: 23197727

Pereira JB, Ossenkoppele R, Palmqvist S, Strandberg TO, Smith R, Westman E, Hansson O. 2019. Amyloid and tau accumulate across distinct spatial networks and are differentially associated with brain connectivity. *eLife* **8**: e50830. DOI: https://doi.org/10.7554/eLife.50830, PMID: 31815669

Pichet Binette A, Gonneaud J, Vogel JW, La Joie R, Rosa-Neto P, Collins DL, Poirier J, Breitner JCS, Villeneuve S, Vachon-Presseau E, Alzheimer's Disease Neuroimaging Initiative, PREVENT-AD Research Group. 2020. Morphometric network differences in ageing versus alzheimer's disease dementia. *Brain* **143**:635–649. DOI: https://doi.org/10.1093/brain/awz414, PMID: 32040564

Pines AR, Cieslak M, Larsen B, Baum GL, Cook PA, Adebimpe A, Dávila DG, Elliott MA, Jirsaraie R, Murtha K, Oathes DJ, Piiwaa K, Rosen AFG, Rush S, Shinohara RT, Bassett DS, Roalf DR, Satterthwaite TD. 2020. Leveraging multi-shell diffusion for studies of brain development in youth and young adulthood. *Developmental Cognitive Neuroscience* **43**:100788. DOI: https://doi.org/10.1016/j.dcn.2020.100788, PMID: 32510347

R Development Core Team. 2020. R: A language and environment for statistical computing. 3.6.3. Vienna, Austria, R Foundation for Statistical Computing. http://www.r-project.org

Racine AM, Adluru N, Alexander AL, Christian BT, Okonkwo OC, Oh J, Cleary CA, Birdsill A, Hillmer AT, Murali D. 2014. Associations between white matter microstructure and amyloid burden in preclinical alzheimer's disease: A multimodal imaging investigation. *NeuroImage. Clinical* **4**:604–614. DOI: https://doi.org/10.1016/j.nicl.2014.02.001

Randolph C, Tierney MC, Mohr E, Chase TN. 1998. The repeatable battery for the assessment of neuropsychological status (RBANS): preliminary clinical validity. *Journal of Clinical and Experimental Neuropsychology* **20**:310–319. DOI: https://doi.org/10.1076/jcen.20.3.310.823, PMID: 9845158

Rheault F, Houde JC, Descoteaux M. 2017. Visualization, interaction and tractometry: dealing with millions of streamlines from diffusion MRI tractography. *Frontiers in Neuroinformatics* **11**:42. DOI: https://doi.org/10.3389/fninf.2017.00042, PMID: 28694776

Rheault F. 2020. *Analyse Et Reconstruction De Faisceaux De La Matière Blanche. in Computer Science*. Université de Sherbrooke.

Rheault F, Poulin P, Valcourt Caron A, St-Onge E, Descoteaux M. 2020. Common misconceptions, hidden biases and modern challenges of dMRI tractography. *Journal of Neural Engineering* **17**:011001. DOI: https://doi.org/10.1088/1741-2552/ab6aad, PMID: 31931484

Rieckmann A, Van Dijk KR, Sperling RA, Johnson KA, Buckner RL, Hedden T. 2016. Accelerated decline in white matter integrity in clinically normal individuals at risk for alzheimer's disease. *Neurobiology of Aging* **42**:177–188. DOI: https://doi.org/10.1016/j.neurobiolaging.2016.03.016, PMID: 27143434

Roy M, Rheault F, Croteau E, Castellano CA, Fortier M, St-Pierre V, Houde JC, Turcotte ÉE, Bocti C, Fulop T, Cunnane SC, Descoteaux M. 2020. Fascicle- and Glucose-Specific deterioration in white matter energy supply in Alzheimer's Disease. *Journal of Alzheimer's Disease* **76**:863–881. DOI: https://doi.org/10.3233/JAD-200213, PMID: 32568202

Sachdev PS, Zhuang L, Braidy N, Wen W. 2013. Is Alzheimer's a disease of the white matter? *Current Opinion in Psychiatry* **26**:244–251. DOI: https://doi.org/10.1097/YCO.0b013e32835ed6e8, PMID: 23493128

Schöll M, Lockhart SN, Schonhaut DR, O'Neil JP, Janabi M, Ossenkoppele R, Baker SL, Vogel JW, Faria J, Schwimmer HD, Rabinovici GD, Jagust WJ. 2016. PET imaging of tau deposition in the aging human brain. *Neuron* **89**:971–982. DOI: https://doi.org/10.1016/j.neuron.2016.01.028, PMID: 26938442

Schultz SA, Strain JF, Adedokun A, Wang Q, Preische O, Kuhle J, Flores S, Keefe S, Dincer A, Ances BM, Berman SB, Brickman AM, Cash DM, Chhatwal J, Cruchaga C, Ewers M, Fox NN, Ghetti B, Goate A, Graff-Radford NR, et al. 2020. Serum neurofilament light chain levels are associated with white matter integrity in autosomal dominant alzheimer's disease. *Neurobiology of Disease* **142**:104960. DOI: https://doi.org/10.1016/j.nbd.2020.104960, PMID: 32522711

Seeley WW, Crawford RK, Zhou J, Miller BL, Greicius MD. 2009. Neurodegenerative diseases target large-scale human brain networks. *Neuron* **62**:42–52. DOI: https://doi.org/10.1016/j.neuron.2009.03.024, PMID: 19376066

Sepulcre J, Schultz AP, Sabuncu M, Gomez-Isla T, Chhatwal J, Becker A, Sperling R, Johnson KA. 2016. In vivo tau, amyloid, and gray matter profiles in the aging brain. *Journal of Neuroscience* **36**:7364–7374. DOI: https://doi.org/10.1523/JNEUROSCI.0639-16.2016, PMID: 27413148

Sepulcre J, Sabuncu MR, Li Q, El Fakhri G, Sperling R, Johnson KA. 2017. Tau and amyloid β proteins distinctively associate to functional network changes in the aging brain. *Alzheimer's & Dementia* **13**:1261–1269. DOI: https://doi.org/10.1016/j.jalz.2017.02.011, PMID: 28366797

Sexton CE, Kalu UG, Filippini N, Mackay CE, Ebmeier KP. 2011. A meta-analysis of diffusion tensor imaging in mild cognitive impairment and Alzheimer's disease. *Neurobiology of Aging* **32**:2322.e5. DOI: https://doi.org/10.1016/j.neurobiolaging.2010.05.019

Song Z, Farrell ME, Chen X, Park DC. 2018. Longitudinal accrual of neocortical amyloid burden is associated with microstructural changes of the fornix in cognitively normal adults. *Neurobiology of Aging* **68**:114–122. DOI: https://doi.org/10.1016/j.neurobiolaging.2018.02.021, PMID: 29602495

Sperling RA, Aisen PS, Beckett LA, Bennett DA, Craft S, Fagan AM, Iwatsubo T, Jack CR, Kaye J, Montine TJ, Park DC, Reiman EM, Rowe CC, Siemers E, Stern Y, Yaffe K, Carrillo MC, Thies B, Morrison-Bogorad M, Wagster MV, et al. 2011. Toward defining the preclinical stages of alzheimer's disease: recommendations from the National Institute on Aging-Alzheimer's Association workgroups on diagnostic guidelines for Alzheimer's disease. *Alzheimer's & Dementia* **7**:280–292. DOI: https://doi.org/10.1016/j.jalz.2011.03.003, PMID: 21514248

Su Y, D'Angelo GM, Vlassenko AG, Zhou G, Snyder AZ, Marcus DS, Blazey TM, Christensen JJ, Vora S, Morris JC, Mintun MA, Benzinger TL. 2013. Quantitative analysis of PiB-PET with FreeSurfer ROIs. *PLOS ONE* **8**: e73377. DOI: https://doi.org/10.1371/journal.pone.0073377, PMID: 24223109

Su Y, Blazey TM, Snyder AZ, Raichle ME, Marcus DS, Ances BM, Bateman RJ, Cairns NJ, Aldea P, Cash L, Christensen JJ, Friedrichsen K, Hornbeck RC, Farrar AM, Owen CJ, Mayeux R, Brickman AM, Klunk W, Price JC, Thompson PM, et al. 2015. Partial volume correction in quantitative amyloid imaging. *NeuroImage* **107**:55–64. DOI: https://doi.org/10.1016/j.neuroimage.2014.11.058, PMID: 25485714

Su Y, Flores S, Wang G, Hornbeck RC, Speidel B, Joseph-Mathurin N, Vlassenko AG, Gordon BA, Koeppe RA, Klunk WE, Jack CR, Farlow MR, Salloway S, Snider BJ, Berman SB, Roberson ED, Brosch J, Jimenez-Velazques I, Dyck CH, Galasko D, et al. 2019. Comparison of Pittsburgh compound B and florbetapir in cross-sectional and longitudinal studies. *Alzheimer's & Dementia: Diagnosis, Assessment & Disease Monitoring* **11**:180–190. DOI: https://doi.org/10.1016/j.dadm.2018.12.008

Theaud G, Houde J-C, Boré A, Rheault F, Morency F, Descoteaux M. 2020a. TractoFlow: a robust, efficient and reproducible diffusion MRIpipeline leveraging nextflow & singularity. *bioRxiv*. DOI: https://doi.org/10.1101/631952

Theaud G. 2020b. TractoFlow-ABS. *GitHub*. https://github.com/scilus/tractoflow-ABS

Tournier JD, Calamante F, Connelly A. 2007. Robust determination of the fibre orientation distribution in diffusion MRI: non-negativity constrained super-resolved spherical deconvolution. *NeuroImage* **35**:1459–1472. DOI: https://doi.org/10.1016/j.neuroimage.2007.02.016, PMID: 17379540

Tournier JD, Smith R, Raffelt D, Tabbara R, Dhollander T, Pietsch M, Christiaens D, Jeurissen B, Yeh CH, Connelly A. 2019. MRtrix3: a fast, flexible and open software framework for medical image processing and visualisation. *NeuroImage* **202**:116137. DOI: https://doi.org/10.1016/j.neuroimage.2019.116137, PMID: 31473352

van der Kant R, Goldstein LSB, Ossenkoppele R. 2020. Amyloid-β-independent regulators of tau pathology in alzheimer disease. *Nature Reviews Neuroscience* **21**:21–35. DOI: https://doi.org/10.1038/s41583-019-0240-3, PMID: 31780819

Villemagne VL, Lopresti BJ, Doré V, Tudorascu D, Ikonomovic MD, Burnham S, Minhas D, Pascoal TA, Mason NS, Snitz B, Aizenstein H, Mathis CA, Lopez O, Rowe CC, Klunk WE, Cohen AD. 2021. What is T+? A gordian knot of tracers, thresholds, and topographies. *Journal of Nuclear Medicine* **62**:614–619. DOI: https://doi.org/10.2967/jnumed.120.245423, PMID: 33384320

Villeneuve S, Rabinovici GD, Cohn-Sheehy BI, Madison C, Ayakta N, Ghosh PM, La Joie R, Arthur-Bentil SK, Vogel JW, Marks SM, Lehmann M, Rosen HJ, Reed B, Olichney J, Boxer AL, Miller BL, Borys E, Jin LW, Huang EJ, Grinberg LT, et al. 2015. Existing pittsburgh Compound-B positron emission tomography thresholds are too high: statistical and pathological evaluation. *Brain* **138**:2020–2033. DOI: https://doi.org/10.1093/brain/awv112, PMID: 25953778

Vipin A, Ng KK, Ji F, Shim HY, Lim JKW, Pasternak O, Zhou JH, Alzheimer's Disease Neuroimaging Initiative. 2019. Amyloid burden accelerates white matter degradation in cognitively normal elderly individuals. *Human Brain Mapping* **40**:2065–2075. DOI: https://doi.org/10.1002/hbm.24507, PMID: 30604903

Vogel JW, Iturria-Medina Y, Strandberg OT, Smith R, Levitis E, Evans AC, Hansson O, Alzheimer's Disease Neuroimaging Initiative, Swedish BioFinder Study. 2020. Spread of pathological tau proteins through communicating neurons in human Alzheimer's disease. *Nature Communications* **11**:2612. DOI: https://doi.org/10.1038/s41467-020-15701-2, PMID: 32457389

Von Der Heide RJ, Skipper LM, Klobusicky E, Olson IR. 2013. Dissecting the uncinate fasciculus: disorders, controversies and a hypothesis. *Brain* **136**:1692–1707. DOI: https://doi.org/10.1093/brain/awt094, PMID: 23649697

Wang Q, Wang Y, Liu J, Sutphen CL, Cruchaga C, Blazey T, Gordon BA, Su Y, Chen C, Shimony JS, Ances BM, Cairns NJ, Fagan AM, Morris JC, Benzinger TLS. 2019. Quantification of white matter cellularity and damage in preclinical and early symptomatic alzheimer's disease. *NeuroImage: Clinical* **22**:101767. DOI: https://doi.org/10.1016/j.nicl.2019.101767, PMID: 30901713

Wassermann D, Makris N, Rathi Y, Shenton M, Kikinis R, Kubicki M, Westin CF. 2016. The white matter query language: a novel approach for describing human white matter anatomy. *Brain Structure and Function* **221**: 4705–4721. DOI: https://doi.org/10.1007/s00429-015-1179-4, PMID: 26754839

Wearn AR, Nurdal V, Saunders-Jennings E, Knight MJ, Isotalus HK, Dillon S, Tsivos D, Kauppinen RA, Coulthard EJ. 2020. T2 heterogeneity: a novel marker of microstructural integrity associated with cognitive decline in people with mild cognitive impairment. *Alzheimer's Research & Therapy* **12**:105. DOI: https://doi.org/10.1186/s13195-020-00672-9, PMID: 32912337

Wen Q, Mustafi SM, Li J, Risacher SL, Tallman E, Brown SA, West JD, Harezlak J, Farlow MR, Unverzagt FW, Gao S, Apostolova LG, Saykin AJ, Wu YC. 2019. White matter alterations in early-stage Alzheimer's disease: A tract-specific study. *Alzheimer's & Dementia: Diagnosis, Assessment & Disease Monitoring* **11**:576–587. DOI: https://doi.org/10.1016/j.dadm.2019.06.003, PMID: 31467968

Zhang X, Sun Y, Li W, Liu B, Wu W, Zhao H, Liu R, Zhang Y, Yin Z, Yu T, Qing Z, Zhu B, Xu Y, Nedelska Z, Hort J, Zhang B, Alzheimer's Disease Neuroimaging Initiative. 2019. Characterization of white matter changes along fibers by automated fiber quantification in the early stages of Alzheimer's disease. *NeuroImage: Clinical* **22**: 101723. DOI: https://doi.org/10.1016/j.nicl.2019.101723, PMID: 30798166

Zhuang L, Sachdev PS, Trollor JN, Kochan NA, Reppermund S, Brodaty H, Wen W. 2012. Microstructural white matter changes in cognitively normal individuals at risk of amnestic MCI. *Neurology* **79**:748–754. DOI: https://doi.org/10.1212/WNL.0b013e3182661f4d, PMID: 22843270

Appendix 1

Supplementary material

```
import FreeSurfer.qry
    #Posterior cingulum
Posterior_Cg.side = only(isthmuscingulate.side or posteriorcingulate.side and (entorhinal.side or fusiform.side or parahippocampal.side or precuneus.side or lingual.side or amygdala.side))
```

Appendix 2

DIAN study group

Last name	First name	Institution	Affiliation	Core	Role	Email address
Allegri	Ricardo	FLENI	FLENI Institute of Neurological Research (Fundacion para la Lucha contra las Enfermedades Neurologicas de la Infancia)	N/A	PI	rallegri@fleni.org.ar
Bateman	Randy	WU	Washington University in St. Louis School of Medicine	Admin	Core leader/PI/ chair	batemanr@wustl.edu
Bechara	Jacob	Sydney	Neuroscience Research Australia	N/A	Site leader	j.bechara@neura.edu.au
Benzinger	Tammie	WU	Washington University in St. Louis School of Medicine	Imaging	Core leader	benzingert@wustl.edu
Berman	Sarah	Pitt	University of Pittsburgh	N/A	PI	bermans@upmc.edu
Bodge	Courtney	Butler	Brown University-Butler Hospital	N/A	Site coordinator	Cbodge@Butler.org
Brandon	Susan	WU	Washington University in St. Louis School of Medicine	Admin/clinical	Core personnel	brandons@wustl.edu
Brooks	William (Bill)	Sydney	Neuroscience Research Australia	N/A	Site coordinator	w.brooks@NeuRA.edu.au
Buck	Jill	IU	Indiana University	N/A	Site coordinator	jilmbuck@iu.edu
Buckles	Virginia	WU	Washington University in St. Louis School of Medicine	Admin	Core personnel	bucklesv@wustl.edu
Chea	Sochenda	Mayo	Mayo Clinic Jacksonville	N/A	Site coordinator	chea.sochenda@mayo.edu
Chhatwal	Jasmeer	BWH	Brigham and Women's Hospital–Massachusetts General Hospital	N/A	PI	Chhatwal.Jasmeer@mgh.harvard.edu
Chrem	Patricio	FLENI	FLENI Institute of Neurological Research (Fundacion para la Lucha contra las Enfermedades Neurologicas de la Infancia)	N/A	Site coordinator	pchremmendez@fleni.org.ar
Chui	Helena	USC	University of Southern California	N/A	PI	helena.chui@med.usc.edu
Cinco	Jake	UCL	University College London	N/A	Site coordinator	jcinco@nhs.net
Cruchaga	Carlos	WU	Washington University in St. Louis School of Medicine	Genetics	Core co-leader	cruchagac@wustl.edu

Continued on next page

continued

Last name	First name	Institution	Affiliation	Core	Role	Email address
Donahue	Tamara	WU	Washington University in St. Louis School of Medicine	N/A	Site coordinator	tammie@wustl.edu
Douglas	Jane	UCL	University College London	N/A	Site coordinator	jdouglas@dementia.ion.ucl.ac.uk
Edigo	Noelia	FLENI	FLENI Institute of Neurological Research (Fundacion para la Lucha contra las Enfermedades Neurologicas de la Infancia)	N/A	Site coordinator	negido@fleni.org.ar
Erekin-Taner	Nilufer	Mayo	Mayo Clinic Jacksonville	N/A	*sub-I*	taner.nilufer@mayo.edu
Fagan	Anne	WU	Washington University in St. Louis School of Medicine	Biomarker	Core leader	fagana@wustl.edu
Farlow	Marty	IU	Indiana University	N/A	PI	mfarlow@iupui.edu
Fitzpatrick	Colleen	BWH	Brigham and Women's Hospital-Massachusetts	N/A	Site co-coordinator	cdfitzpatrick@bwh.harvard.edu
Flynn	Gigi	WU	Washington University in St. Louis School of Medicine	Admin/ Clinical	Core personnel	flynng@wustl.edu
Fox	Nick	UCL	University College London	N/A	PI	nfox@dementia.ion.ucl.ac.uk
Franklin	Erin	WU	Washington University in St. Louis School of Medicine	Neuropath	Core coordinator	efranklin@wustl.edu
Fujii	Hisako	Japan	Osaka City University	N/A	Assistant/ coord	hfujii@med.osaka-cu.ac.jp
Gant	Cortaiga	WU	Washington University in St. Louis School of Medicine	Admin/ Clinical	Core personnel	cortaiga.gant@wustl.edu
Gardener	Samantha	Perth	Edith Cowan University, Perth	N/A	Site coordinator	s.gardener@ecu.edu.au
Ghetti	Bernardino	IU	Indiana University	N/A	*sub-I*	bghetti@iupui.edu
Goate	Alison	Icahn NY	Icahn School of Medicine at Mount Sinai	Genetics	Core co-leader	alison.goate@mssm.edu
Goldman	Jill	CU	Columbia University	N/A	Genetics ethics	JG2673@cumc.columbia.edu
Gordon	Brian	WU	Washington University in St. Louis School of Medicine	Imaging	Core personnel	bagordon@wustl.edu
Graff-Radford	Neill	Mayo	Mayo Clinic Jacksonville	N/A	PI	graffradford.neill@mayo.edu

Continued on next page

continued

Last name	First name	Institution	Affiliation	Core	Role	Email address
Gray	Julia	WU	Washington University in St. Louis School of Medicine	Biomarker	Core personnel	gray@wustl.edu
Groves	Alexander	WU	Washington University in St. Louis School of Medicine	Biomarker	Core coordinator	amgroves@wustl.edu
Hassenstab	Jason	WU	Washington University in St. Louis School of Medicine	Clinical	Core personnel	hassenstabj@wustl.edu
Hoechst-Swisher	Laura	WU	Washington University in St. Louis School of Medicine	Admin/clinical	Core coordinator	goodl@wustl.edu
Holtzman	David	WU	Washington University in St. Louis School of Medicine	N/A	Associate director	holtzman@wustl.edu
Hornbeck	Russ	WU	Washington University in St. Louis School of Medicine	Imaging	Core coordinator	russ@wustl.edu
Houeland DiBari	Siri	Munich	German Center for Neurodegenerative Diseases (DZNE) Munich	N/A	Site coordinator	Siri.HouelandDiBari@dzne.de
Ikeuchi	Takeshi	Niigata	Niigata University	N/A	*Site leader*	ikeuchi@bri.niigata-u.ac.jp
Ikonomovic	Snezana	Pitt	University of Pittsburgh	N/A	Site coordinator	ikonomovics@upmc.edu
Jack	Clifford	Mayo	Mayo Clinic Jacksonville	MRI QC	Vendor MRI QC	jack.clifford@mayo.edu
Jerome	Gina	WU	Washington University in St. Louis School of Medicine	Biomarker	Core coordinator	ginajerome@wustl.edu
Jucker	Mathias	Tubingen	German Center for Neurodegnerative Diseases (DZNE) Tubingen	N/A	PI	mathias.jucker@uni-tuebingen.de
Karch	Celeste	WU	Washington University in St. Louis School of Medicine	Administrative	Core personnel	karchc@wustl.edu
Kasuga	Kensaku	Niigata	Niigata University	N/A	Site coordinator	ken39@bri.niigata-u.ac.jp
Kawarabayashi	Takeshi	Hirosaki	Hirosaki University	N/A	Clinician	tkawara@hirosaki-u.ac.jp
Klunk	William (Bill)	Pitt	University of Pittsburgh	N/A	sub-I	klunkwe@gmail.com
Koeppe	Robert	U of Michigan	University of Michigan	PET QC	Vendor PET QC	koeppe@umich.edu

Continued on next page

continued

Last name	First name	Institution	Affiliation	Core	Role	Email address
Kuder-Buletta	Elke	Tubingen	German Center for Neurodegnerative Diseases (DZNE) Tubingen	N/A	Site coordinator	elke.buletta@med.uni-tuebingen.de
Laske	Christoph	Tubingen	German Center for Neurodegnerative Diseases (DZNE) Tubingen	N/A	*sub-I*	christoph.laske@med.uni-tuebingen.de
Lee	Jae-Hong	Korea	Asan Medical Center	N/A	PI	jhlee@amc.seoul.kr
Levin	Johannes	Munich	German Center for Neurodegnerative Diseases (DZNE) Munich	N/A	PI	Johannes.Levin@med.uni-muenchen.de
Martins	Ralph	Perth	Edith Cowan University	N/A	PI	r.martins@ecu.edu.au
Mason	Neal Scott	UPMC	University of Pittsburgh Medical Center	PIB QC	Vendor PIB QC	masonss@upmc.edu
Masters	Colin	Melb	University of Melbourne	N/A	PI – former	c.masters@unimelb.edu.au
Maue-Dreyfus	Denise	WU	Washington University in St. Louis School of Medicine	Clinical	Core personnel	dmdreyfu@wustl.edu
McDade	Eric	WU	Washington University in St. Louis School of Medicine	Clinical	Core leader assoc	ericmcdade@wustl.edu
Mori	Hiroshi	Japan	Osaka City University	N/A	PI	mori@med.osaka-cu.ac.jp
Morris	John	WU	Washington University in St. Louis School of Medicine	Clinical	Core leader	jcmorris@wustl.edu
Nagamatsu	Akem	Tokyo	Tokyo University	N/A	Site coordinator	akm77-tky@umin.ac.jp
Neimeyer	Katie	CU	Columbia University	N/A	Site coordinator	kn2416@cumc.columbia.edu
Noble	James	CU	Columbia University	N/A	PI	jn2054@columbia.edu
Norton	Joanne	WU	Washington University in St. Louis School of Medicine	Genetics	Core coordinator	nortonj@wustl.edu
Perrin	Richard	WU	Washington University in St. Louis School of Medicine	Neuropath	Core leader	rperrin@wustl.edu
Raichle	Marc	WU	Washington University in St. Louis School of Medicine	Imaging	Core personnel	mraichle@wustl.edu
Renton	Alan	Icahn NY	Icahn School of Medicine at Mount Sinai	Genetics	Core personnel	alan.renton@mssm.edu

Continued on next page

continued

Last name	First name	Institution	Affiliation	Core	Role	Email address
Ringman	John	USC	University of Southern California	N/A	*sub-I*	john.ringman@med.usc.edu
Roh	Jee Hoon	Korea	Asan Medical Center	N/A	*sub-I*	roh@amc.seoul.kr
Salloway	Stephen	Butler	Brown University-Butler Hospital	N/A	PI	SSalloway@Butler.org
Schofield	Peter	Sydney	Neuroscience Research Australia	N/A	PI	p.schofield@neura.edu.au
Shimada	Hiroyuki	Osaka	Osaka City University	N/A	*Site leader*	h.shimada@med.osaka-cu.ac.jp
Sigurdson	Wendy	WU	Washington University in St. Louis School of Medicine	N/A	Site coordinator	sigurdsonw@wustl.edu
Sohrabi	Hamid	Perth	Edith Cowan University	N/A	Site coordinator	h.sohrabi@ecu.edu.au
Sparks	Paige	BWH	Brigham and Women's Hospital-Massachusetts	N/A	Site coordinator	kpsparks@bwh.harvard.edu
Suzuki	Kazushi	Tokyo	Tokyo University	N/A	*Site leader*	kazusuzuki-tky@umin.ac.jp
Taddei	Kevin	Perth	Edith Cowan University	N/A	Site coordinator	k.taddei@ecu.edu.au
Wang	Peter	WU	Washington University in St. Louis School of Medicine	Biostat	Core coordinator	guoqiao@wustl.edu
Xiong	Chengjie	WU	Washington University in St. Louis School of Medicine	Biostat	Core leader	chengjie@wustl.edu
Xu	Xiong	WU	Washington University in St. Louis School of Medicine	Biostat	Core personnel	xxu@wustl.edu
Levey	Allan	Emory	Emory University School of Medicine	N/A	Project leader	alevey@emory.edu